Article

Cell Metabolism

A Cell-Autonomous Mammalian 12 hr Clock Coordinates Metabolic and Stress Rhythms

Graphical Abstract

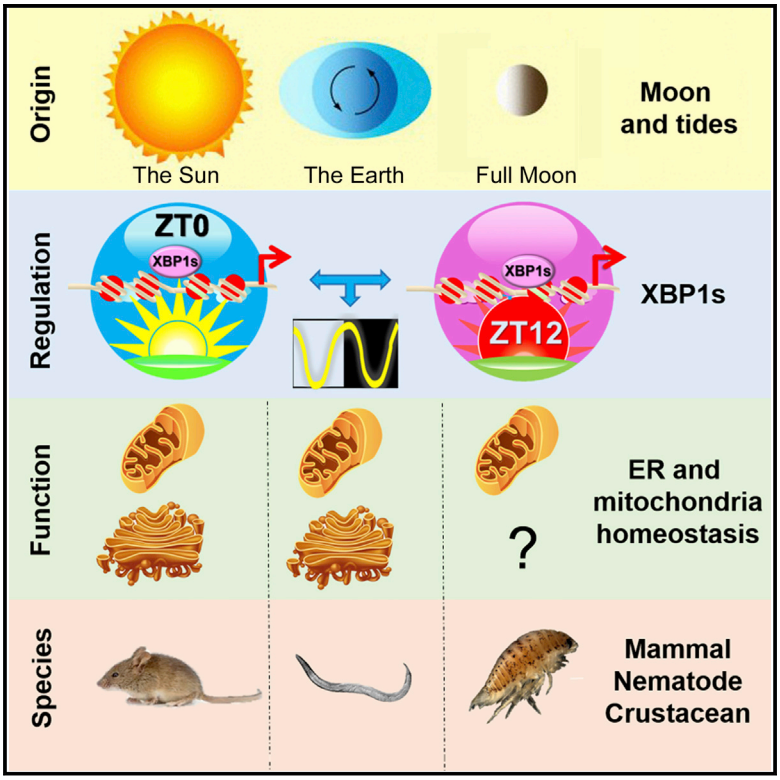

Authors

Bokai Zhu, Qiang Zhang, Yinghong Pan, ..., Athanasios C. Antoulas, Clifford C. Dacso, Bert W. O'Malley

Correspondence

berto@bcm.edu

In Brief

Besides circadian rhythms, oscillations with ~12 hr period exist, but their origin, regulation, and function remain elusive. Zhu et al. show that a cell-autonomous 12 hr clock functions independently from the circadian clock to coordinate ER and mitochondria functions. The 12 hr clock is conserved in nematodes, crustaceans, and mammals and likely circatidal in origin.

Highlights

- Hepatic 12 hr rhythms are prevalent in ER and mitochondria homeostasis genes
- Cell-autonomous 12 hr rhythms are independent of the circadian clock
- The 12 hr rhythm of gene expression is transcriptionally regulated by XBP1s
- Mammalian 12 hr rhythms of gene expression are conserved in crustaceans and nematodes

Zhu et al., 2017, Cell Metabolism *25*, 1305–1319
June 6, 2017
http://dx.doi.org/10.1016/j.cmet.2017.05.004

Cell Metabolism
Article

A Cell-Autonomous Mammalian 12 hr Clock Coordinates Metabolic and Stress Rhythms

Bokai Zhu,[1] Qiang Zhang,[5] Yinghong Pan,[6] Emily M. Mace,[2] Brian York,[1,4] Athanasios C. Antoulas,[1,5,7] Clifford C. Dacso,[1,3,4,5,8] and Bert W. O'Malley[1,4,8,9,*]
[1]Department of Molecular and Cellular Biology
[2]Department of Pediatrics
[3]Department of Medicine
[4]Dan L. Duncan Cancer Center
Baylor College of Medicine, Houston, TX 77030, USA
[5]Department of Electrical and Computer Engineering, Rice University, Houston, TX 77005, USA
[6]Department of Biology and Biochemistry, University of Houston, Houston, TX 77004, USA
[7]Max Planck Fellow Group for Data-Driven System Reduction and Identification, Max Planck Institute for Dynamics of Complex Technical Systems, Magdeburg 39106, Germany
[8]These authors contributed equally
[9]Lead Contact
*Correspondence: berto@bcm.edu
http://dx.doi.org/10.1016/j.cmet.2017.05.004

SUMMARY

Besides circadian rhythms, oscillations cycling with a 12 hr period exist. However, the prevalence, origin, regulation, and function of mammalian 12 hr rhythms remain elusive. Utilizing an unbiased mathematical approach identifying all superimposed oscillations, we uncovered prevalent 12 hr gene expression and metabolic rhythms in mouse liver, coupled with a physiological 12 hr unfolded protein response oscillation. The mammalian 12 hr rhythm is cell autonomous, driven by a dedicated 12 hr pacemaker distinct from the circadian clock, and can be entrained in vitro by metabolic and ER stress cues. Mechanistically, we identified XBP1s as a transcriptional regulator of the mammalian 12 hr clock. Downregulation of the 12 hr gene expression strongly correlates with human hepatic steatosis and steatohepatitis, implying its importance in maintaining metabolic homeostasis. The mammalian 12 hr rhythm of gene expression also is conserved in nematodes and crustaceans, indicating an ancient origin of the 12 hr clock. Our work sheds new light on how perturbed biological rhythms contribute to human disease.

INTRODUCTION

In addition to the well-characterized 24 hr circadian rhythm, biological rhythms that cycle with shorter periods also exist (Hughes et al., 2009). For example, marine animals of the coastal regions harbor a dominant circatidal clock tuned to the ~12 hr ebb and flow of the tides (Wilcockson and Zhang, 2008). A small cluster of genes cycling with a 12 hr period was identified in several peripheral murine tissues (Hoogerwerf et al., 2008; Hughes et al., 2009; Zhang et al., 2014). In humans, body temperature, blood pressure, cognitive performance, circulating hormones, and sleep patterns all exhibit 12 hr rhythms (Ayala et al., 1990; Bjerner et al., 1955; Broughton and Mullington, 1992; Colquhoun et al., 1978). Altered 12 hr rhythms also were reported in human diseases (Haus et al., 2001; Otsuka et al., 1997). These data collectively imply that the 12 hr rhythm is potentially important for systemic homeostasis, and its dysregulation may lead to the development and progression of metabolic diseases.

Among these 12 hr cycling genes, the most intriguing discovery was the identification of ~200 genes cycling with a 12 hr period in mouse liver (Hughes et al., 2009). However, since the COSOPT method used to identify 12 hr cycling transcripts in this study requires the user to pre-assign a period range (Refinetti et al., 2007), only dominant 12 hr genes were identified. Thus, 200 significantly underestimates the true prevalence of 12 hr cycling genes, as the vast majority are likely to be superimposed by other oscillations and thus evade detection.

To be able to comprehensively identify novel genes with superimposed 12 hr rhythms, we employed an unbiased mathematical approach called the "eigenvalue/pencil" method to identify all superimposed oscillations from high-resolution time series data and identified a total of 3,652 hepatic genes with 12 hr rhythms. These genes are enriched in endoplasmic reticulum (ER) and mitochondria metabolism and quality control pathways, indicating that the mammalian 12 hr clock orchestrates Coordinated Rhythms of ER and Mitochondria Actions (CREMA). We further demonstrated that a dedicated 12 hr pacemaker distinct from the circadian clock in mammalian cells controls the majority of 12 hr rhythmic gene expression and metabolism. The 12 hr rhythm of gene expression is cell autonomous and can be established in vitro in response to metabolic stress and/or ER stress cues, and loss of 12 hr cycling gene expression strongly correlates with progression to nonalcoholic fatty liver disease (NAFLD) in humans. Mechanistically, we identified the spliced form of XBP1 (XBP1s), an unfolded protein response (UPR) transcription factor (TF), as a key transcriptional regulator of the 12 hr rhythm. Intriguingly, the 12 hr rhythms of UPR and metabolic gene

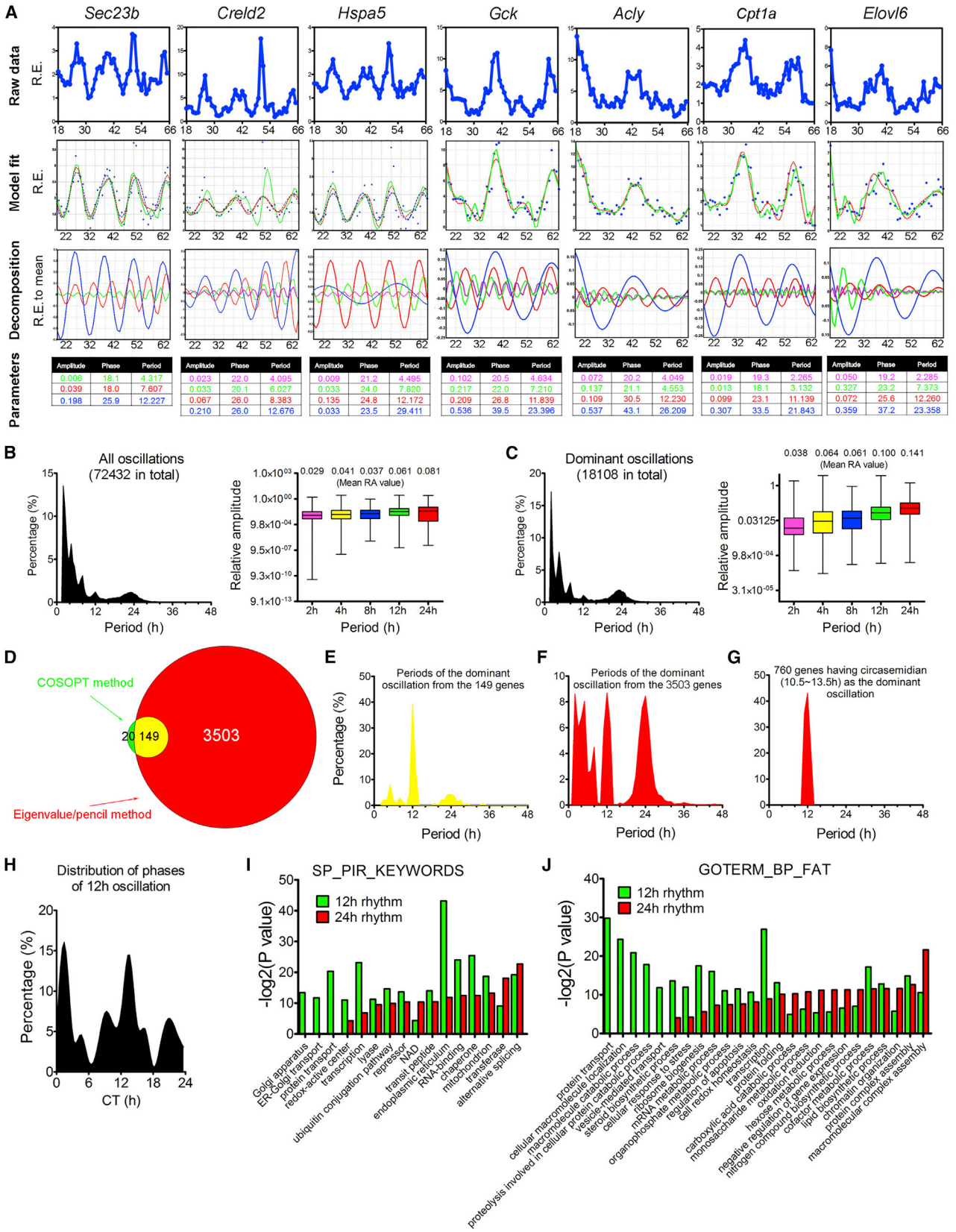

(legend on next page)

expression are evolutionarily conserved in nematodes. Moreover, the 12 hr rhythm of mitochondrial DNA (mtDNA)-encoded gene transcription, which was previously only found in marine crustaceans harboring circatidal rhythms, also is conserved in mammals and nematodes, suggesting strongly that the 12 hr clock has an ancient origin.

RESULTS

The Eigenvalue/Pencil Method Identifies All Superimposed Biological Oscillations in an Unbiased Manner

To comprehensively identify both dominant and superimposed biological oscillations in an unbiased manner, we utilized an eigenvalue/pencil approach that was previously developed for spectrum analysis in the digital signal processing field. Exerting no constraints on periods, it permits the unbiased identification of various superimposed periodic oscillations from a given time series dataset. We initially applied our approach to a high-resolution hepatic gene expression microarray from mice kept under constant darkness (analyzed at 1 hr intervals for 48 hr) (Hughes et al., 2009) and analyzed a total of 18,108 hepatic genes.

The vast majority of oscillations identified were circadian rhythms and oscillations that cycle at different harmonics (~12 hr, 8 hr, 4 hr, etc.) of the circadian rhythm (Figures 1A–1C; Table S1). We identified a total of 5,005 genes with circadian rhythms, including all known core clock genes, which is a significant increase compared to an earlier study using the COSOPT method (Hughes et al., 2009) (Figures S1A–S1E). For the 3,519 newly identified circadian genes, a significant portion are superimposed by other dominant oscillations of smaller periods (Figure S1D), thus circumventing detection by the original method. Importantly, genes with superimposed circadian rhythms reveal drastically altered cycling patterns in *BMAL1*$^{-/-}$ mice (*BMAL1* knockout [KO]) (Yang et al., 2016) (Figure S1F), while genes without superimposed circadian rhythm exhibit similar diurnal gene expression profiles between wild-type (WT) and *BMAL1* KO mice, with examples including *Eif2ak3* (also known as *Perk*) and *Gmppb* (Figure S1G). Further, our method demonstrates that their unique oscillatory patterns are largely composed of three oscillations with periods of ~12 hr, 8 hr, and 6 hr (Figure S1G). Finally, by comparing oscillations identified from different microarray probes against the same gene (Figures S2A–S2C), we concluded that oscillations with periods of ~12 hr and ~8 hr also are robust rhythms with potential biological significance. Taken together, these results indicate that our eigenvalue/pencil method can accurately identify superimposed oscillations from high-resolution microarray in an unbiased manner.

Prevalent Hepatic 12 hr mRNA Oscillation of Metabolism and ER Stress/UPR Genes

In addition to circadian genes, we identified a total of 3,652 (20%) and 6,294 (35%) genes having ~12 hr and 8 hr oscillations (Tables S1 and S2), respectively, significantly expanding their repertoires compared to the previous study (Hughes et al., 2009) (Figures 1D–1G; Figures S2D–S2G). Our method also outperforms JTK_CYCLE (Hughes et al., 2010), ARSER (Yang and Su, 2010), and RAIN (Thaben and Westermark, 2014) methods in robustly uncovering novel genes with superimposed 12 hr rhythms (Figures S2H–S2S; Table S3). Of these 12 hr and 8 hr genes, 760 and 1,430 of them are dominant (whose 12 hr or 8 hr amplitudes are the greatest among all identified oscillations) (Figure 1G; Figure S2G; Table S2). Overall, the average amplitude gradually decreases with shorter periods, with those of 12 hr oscillations exhibiting the second largest amplitude (Figures 1B and 1C).

We focused on the 12 hr rhythms due to their unexpected prevalence. The phases of 12 hr rhythms are heavily restricted to dawn (CT0) and dusk (CT12) (Figure 1H), contrasting with the evenly distributed phases of circadian rhythm (Koike et al., 2012). Gene Ontology (GO) terms preferentially associated with 12 hr genes are highly enriched for ER- and metabolism-related biological pathways (Figures 1I and 1J; Figure S2T; Table S4). While 12 hr are often the dominant oscillations in ER-related genes, 12 hr cycling metabolism genes often have superimposed circadian rhythms (Table S2). It is worth mentioning that these GO terms are not mutually exclusive, and a significant number of metabolism genes are known to be involved in ER homeostasis and vice versa (Wang et al., 2011). Overall, we identified a total of 91 key ER/metabolism genes (Table S2) with 12 hr amplitude greater than 0.1. These results collectively demonstrate that the 12 hr rhythm of gene expression is far more prevalent than was initially appreciated, and one of the major functions of the 12 hr rhythms is to coordinate ER stress/UPR with metabolism to ensure systemic homeostasis in metabolic tissues.

12 hr Rhythms of ER/Metabolism Genes Are Independent from the Circadian Clock

The relationship of the 12 hr rhythm with circadian rhythm represents a central unanswered question. In theory, the 12 hr rhythm either can be established by two circadian transcription activators or repressors appearing in anti-phase (Westermark and

Figure 1. The Eigenvalue/Pencil Method Reveals Prevalence of 12 hr Hepatic mRNA Oscillations

(A) Decomposition of gene oscillations by the eigenvalue/pencil method. Top row: raw microarray data; second row: fitting two different models (fifth-order approximation in dashed red and ninth-order approximation in solid green) to raw data (blue dots); third row: superimposed oscillations revealed by the ninth-order approximation; fourth row: amplitudes, phases, and periods of different oscillations with the color matching the different oscillations depicted in the third row.

(B and C) The distribution of periods (left) and average amplitudes (right) of all (B) or dominant (C) oscillations identified. Box plots in (B) and (C) are graphed as minimum to maximum.

(D) Venn diagram comparison of the number of 12 hr genes identified via the eigenvalue/pencil or the COSOPT method.

(E–G) The distributions of periods of the dominant oscillations from the 149 commonly found 12 hr genes (E), the 3,503 12 hr genes only identified by the eigenvalue method (F), or the 760 dominant 12 hr genes identified by the eigenvalue method (G).

(H) The distribution of phases of all 12 hr genes identified by the eigenvalue approach.

(I and J) GO analyses revealing top-enriched SP_PIR_KEYWORDS (I) or GOTERM_BP_FAT (J) terms in all 12 hr and circadian genes identified by the eigenvalue approach.

Herzel, 2013) or can be established by "separate" 12 hr clock machinery independent from the circadian clock. To distinguish between these two possibilities, we first examined the mathematical relationships among the three most prominent oscillations identified from each of the 91 ER/metabolism genes with strong 12 hr rhythms. The angles among different oscillations are approximately 90° in most situations, suggesting that the 12 hr oscillation (and also 8 hr oscillation) is largely mathematically independent from the circadian rhythm (Table S2). To verify the mathematical results empirically, we analyzed mouse hepatic RNA sequencing (RNA-seq) from WT and *BMAL1* KO mice for these 91 genes under constant darkness conditions (Yang et al., 2016). We reasoned that if the 12 hr rhythm is independent from the circadian clock, one would expect to observe more discernible 12 hr rhythms of gene expression in *BMAL1* KO mice. We classified these 91 genes into four clusters based upon whether the superimposed 12 hr rhythm is dominant or not. For the 51 dominant 12 hr genes, all but 7 (Figure 2A, cluster II) revealed perceptible ~12 hr rhythms in *BMAL1* KO mice (i.e., *Acly* and *Ddit3*; Figure 2B). For the 40 remaining 12 hr non-dominant genes, 17 lack superimposed circadian rhythms (Figure 2A, cluster III), and their gene expression profiles are similar between WT and *BMAL1* KO mice (i.e., *Eif2ak3*, Figure S1G; *Pparg*, Figure 2B). The remaining 23 genes have non-dominant 12 hr rhythms superimposed with both circadian rhythms and other oscillations of smaller periods (Figure 2A, cluster IV). Thus, in *BMAL1* KO mice, the expression profiles often exhibited two non-symmetrical peaks within one diurnal cycle (i.e., *Fasn* and *Gck*; Figure 2B), consistent with the superimposition patterns of 12 hr rhythms and oscillations of smaller periods. As an important control, we failed to observe discernible 12 hr rhythms of gene expression in *BMAL1* KO mice for genes lacking 12 hr rhythms in WT mice (Figure S3A). The independent relationship between 12 hr and 24 hr rhythms is (1) further validated in *CLOCK* mutant mice (Miller et al., 2007) (Figures S3B and S3C) and (2) supported by the spatial segregation of 12 hr and 24 hr cycling enhancer RNAs (eRNAs) for genes harboring superimposed 24 hr and 12 hr mRNA oscillations (Fang et al., 2014) (Figures S3D–S3F). These observations demonstrate that the 12 hr rhythm of gene expression, especially those involved in ER/metabolic pathways, is driven by a dedicated 12 hr pacemaker that is distinct from the circadian clock in mammalian cells.

The 12 hr Rhythm of Gene Expression Can Be Established by Metabolic and ER Stress Cues In Vitro

Our findings raise an important question: can the 12 hr rhythm of gene expression be found in vitro or does its establishment require systemic cues only found in vivo as previously suggested (Cretenet et al., 2010; Hughes et al., 2009)? Applying the eigenvalue/pencil method to a high-resolution microarray of NIH 3T3 cells synchronized by forskolin (Hughes et al., 2009) revealed no 12 hr rhythms in vitro (Figure S4A). While these data may simply imply that the 12 hr rhythm of gene expression is not found in vitro, an alternative explanation is that forskolin is only capable of synchronizing the circadian clock but not the circadian clock-independent 12 hr clock; therefore, the 12 hr rhythm is not observed in vitro in this study.

To seek evidence supporting the latter hypothesis, we searched for other chemical "cues" that may synchronize the 12 hr clock in vitro. Since the 12 hr genes are enriched in UPR pathways, we speculated that treating cells transiently with an ER stress inducer tunicamycin (Tu) might establish the 12 hr mRNA rhythms. Of the six genes that are responsive to Tu (Figures S4B and S4D), a 2 hr Tu shock (25 ng/mL) is sufficient to establish robust 12 hr mRNA oscillations in mouse embryonic fibroblasts (MEFs), which can persist for at least 48 hr after the initial induction (Figure 3A). The phase and amplitude of 12 hr mRNA oscillations are dependent on the dose of Tu (Figure S4E). The 12 hr oscillations of gene expression in vitro also are independent from the circadian clock as *Bmal1* ablation fails to affect their 12 hr rhythms (Figure 3B; Figures S4F and S4H). These data are consistent with the observation that a 2 hr Tu induction fails to establish the circadian clock in MEFs (Figure S4C).

We expanded our search for other 12 hr clock-synchronizing cues that are more physiologically relevant than Tu. Because of the strong enrichment of metabolic genes with 12 hr rhythms, we reasoned that a transient metabolic stress, like glucose depletion (GD) or 2-deoxy-D-glucose (2-DG) treatment, which also leads to ER stress (Xu et al., 2005), may be sufficient to establish the 12 hr rhythms. As expected, a 2 hr GD or 2-DG treatment establishes the 12 hr rhythms of genes involved in glucose and fatty acid metabolism, such as *Gfpt1* and *Acly* (Figures 3C and 3D). GD and 2-DG also established the 12 hr rhythm of UPR gene *Eif2ak3* (Figures 3C and 3D). Despite smaller amplitudes, GD also can establish circadian oscillation of core circadian clock genes *Bmal1* and *Rev-erbα* with similar phases compared to Dex-induced rhythms (Figures S4I and S4J). GD-induced 12 hr rhythms are also independent of the circadian clock (Figure 3E; Figure S4J).

To further confirm these qPCR results, we generated a MEF line stably expressing destabilized luciferase driven by a 1 kb *Eif2ak3* promoter (*Eif2ak3*-dluc) and subjected the cells to real-time luminescence recording. As shown in Figures 3F–3H, a 2 hr Tu or GD treatment, but not vehicle or mock treatment, is sufficient to establish the robust ~12 hr rhythm of luciferase activity, with Tu being a stronger zeitgeber than GD (Figure 3J). We calculated the period of *Eif2ak3*-dluc oscillation as 12.56 ± 0.10 hr (mean ± SEM) (Figure 3I). These data further suggest that by regulating genes involved in metabolism and UPR and responding to metabolic and ER stress cues, the mammalian 12 hr clock functions to coordinate physiologically dynamic metabolic and ER stress rhythms.

The Mammalian 12 hr Rhythm of Gene Expression Is Cell Autonomous

We next addressed whether the observed 12 hr rhythm in vitro is cell autonomous. We generated another MEF line stably expressing destabilized GFP (dGFP) driven by the same 1 kb *Eif2ak3* promoter (*Eif2ak3*-dGFP) and subjected these cells to time-lapse microscopy in the absence of external cues. Although, during the imaging, the cells were cultured in serum-free medium, we still observed cell proliferation (Figure 4), likely because the parental MEFs were previously immortalized by SV40 and resistant to serum starvation-induced cell cycle arrest (Stashi et al., 2014). For rapidly proliferating cells (doubling time < 20 hr), we decided to quantify the combined dGFP intensities of the daughter (and granddaughter) cells arising from the same original single cell after every cell division event (termed cell

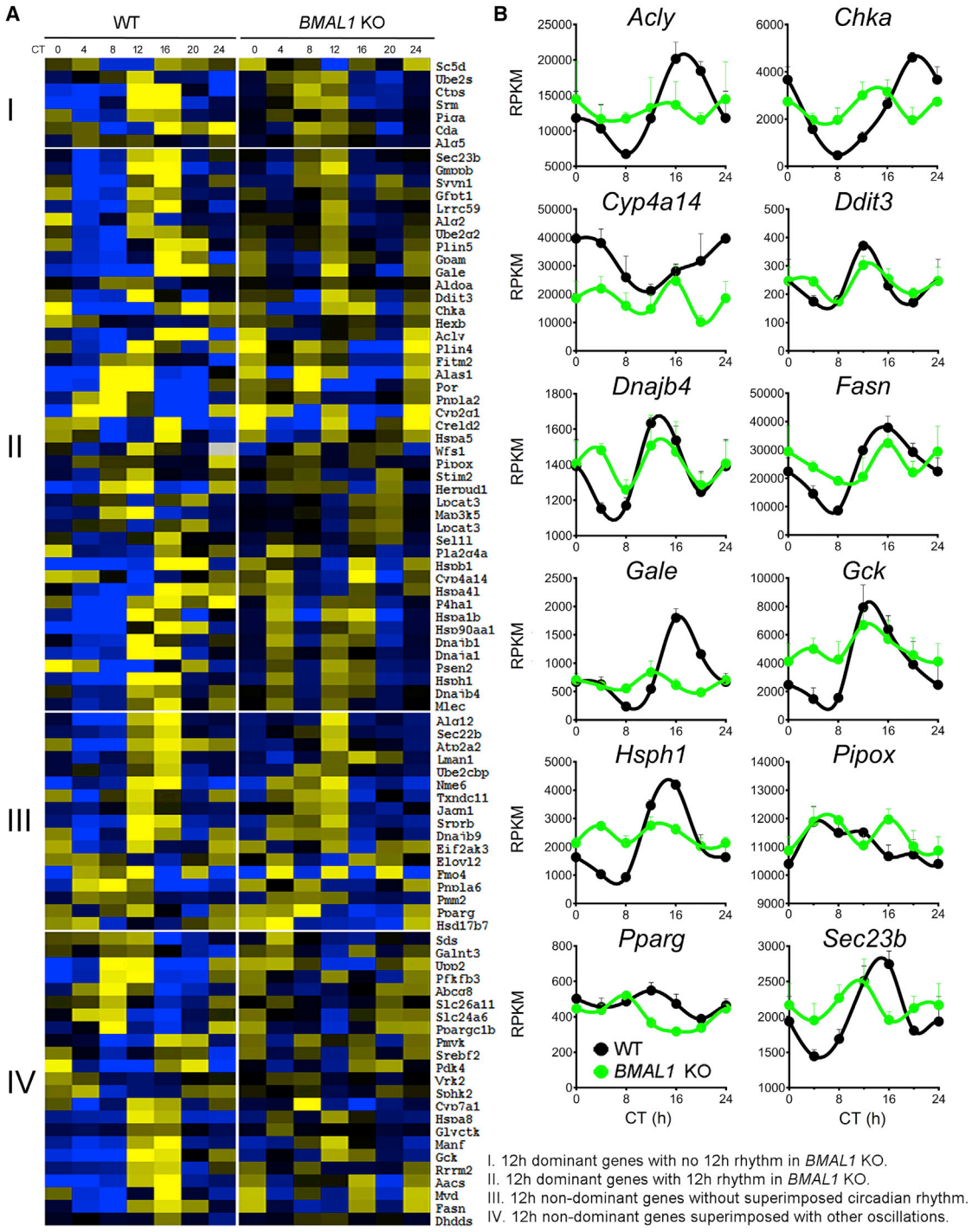

Figure 2. Hepatic 12 hr Oscillations Are Independent from the Circadian Clock

Heatmap (A) and representative RPKM normalized gene expression (B) from WT and *BMAL1* KO mouse under constant darkness conditions. Data are graphed as the mean ± SEM (n = 4).

lineages). After mathematically correcting for the baseline dGFP changes, we observed a robust ~12 hr period of dGFP oscillation in single cell lineages (Figures 4A–4F; Figure S4K; Movie S1). Intriguingly, the ~12 hr rhythm of dGFP oscillation in daughter cells is not reset by the cell divisions, and the phases of oscillations are synchronized between the two daughter cells as well (Figures 4A–4C; Movie S1), which further justifies our method of tracking the whole cell lineages following cell divisions. Of a total of 89 single cell lineage recordings, the period of most dominant *Eif2ak3*-dGFP oscillations centered around

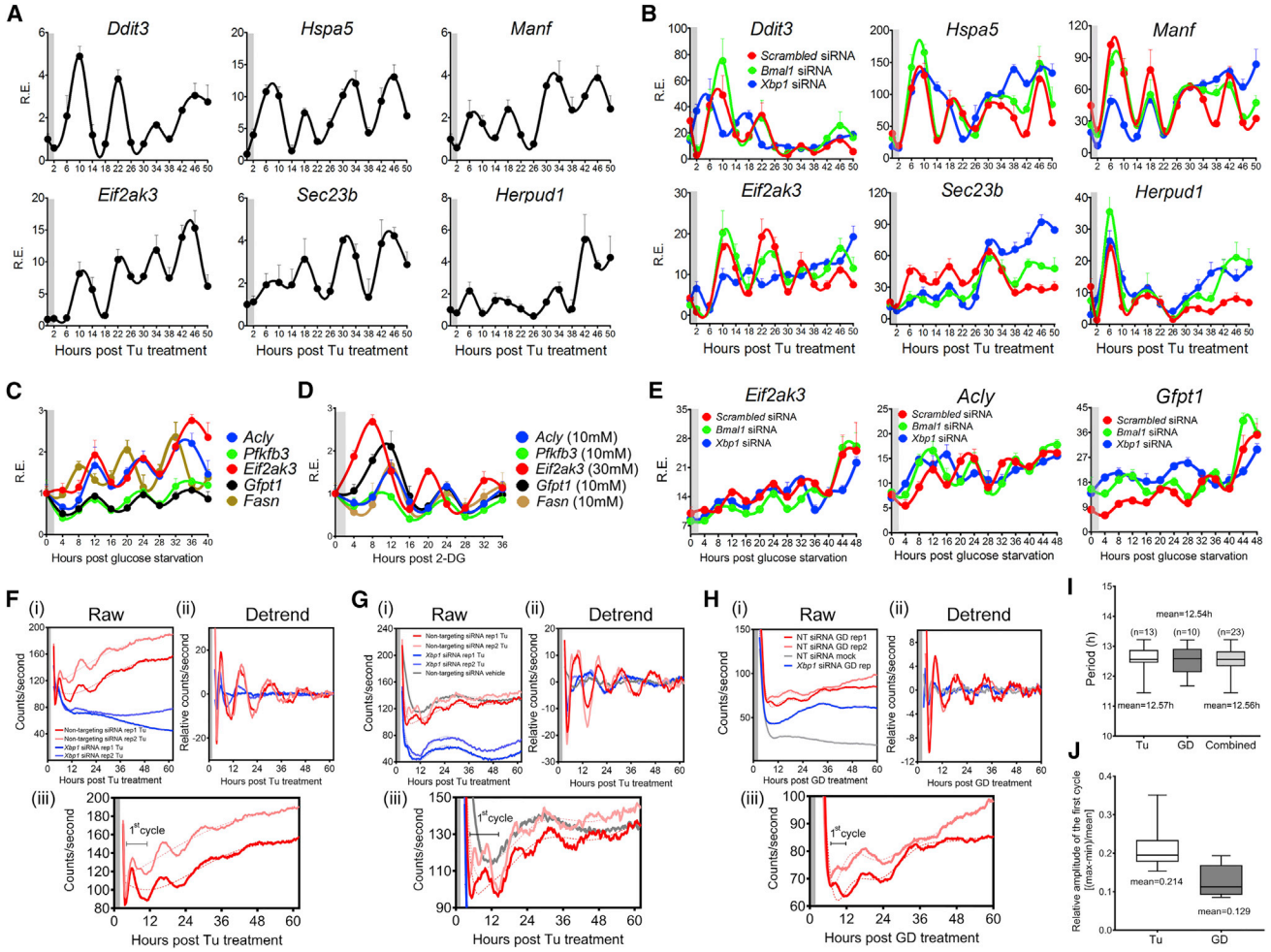

Figure 3. 12 hr Rhythm of Gene Expression Can Be Synchronized by ER and Metabolic Stress Cues

(A and B) MEFs were treated with Tu (A) or were transfected with different siRNAs and treated with Tu (B), and qPCR was performed post-Tu.

(C and D) MEFs were glucose depleted (C) or treated with different concentrations of 2-DG (D) for 2 hr, and qPCR was performed post-GD or post-2-DG.

(E) MEFs were transfected with different siRNAs and glucose depleted for 2 hr, and qPCR was performed post-GD.

(F–J) Real-time luminescence recording of non-targeting or *Xbp1* siRNA-transfected *Eif2ak3*-dluc MEFs in response to vehicle (mock) control, Tu (F and G) or glucose depletion treatment (H). Raw (i), detrended (ii), and magnified graphs (iii) are provided. For Tu treatment, two independent experiments are shown. Gray boxes indicate the duration of treatment. Calculated periods of Tu, GD-entrained, and combined oscillations (I). Relative amplitudes of the first cycle in Tu and GD-entrained oscillations (J). Data are graphed as the mean ± SEM (n = 3) for qPCR.

~12 hr (Figure 4G), and the period of cell-autonomous *Eif2ak3*-dGFP oscillation was calculated to be 12.59 ± 0.11 hr (mean ± SEM), consistent with population luminescence results. Further, the average amplitudes of cell-autonomous 12 hr *Eif2ak3*-dGFP oscillation is 0.2571 (Figure S4L), larger than that of Tu or GD-entrained population amplitudes. Superimposed oscillations with smaller amplitudes were also identified from single cell recordings that cycle with periods of 8.45 ± 0.08 hr and 6.45 ± 0.06 hr, respectively. Intriguingly, these periods are consistent with the decomposition results of hepatic *Eif2ak3* expression in vivo (Figure S1G).

Prevalence of 12 hr Rhythm of Hepatic Protein Expression

In addition to the prevalence of 12 hr mRNA rhythms, we also identified 434 (~15%) hepatic proteins cycling with a period of ~12 hr by analyzing a published time series hepatic proteomics dataset (Robles et al., 2014) (Figure S5A). A limited ~35% overlap with 12 hr cycling mRNAs indicates that both transcriptional and post-transcriptional controls contribute to the regulation of 12 hr rhythms of hepatic gene expression (Table S5), which is consistent with the known limited overlap between hepatic 24 hr cycling mRNA and proteins (Robles et al., 2014). GO analysis of 12 hr cycling proteins revealed strong enrichment of ER and, intriguingly, mitochondria-associated metabolism pathways (Figure 5A; Figures S5B and S5C; Table S5). In light of these findings, we coined the term Coordinated Rhythms of ER and Mitochondria Actions (CREMA) to reflect the coupled rhythmic actions of the two organelles in maintaining systemic metabolic homeostasis and stress response (Figure S6A). We validated several of their 12 hr rhythms by high-resolution immunoblot analysis (Figures S5D–S5F).

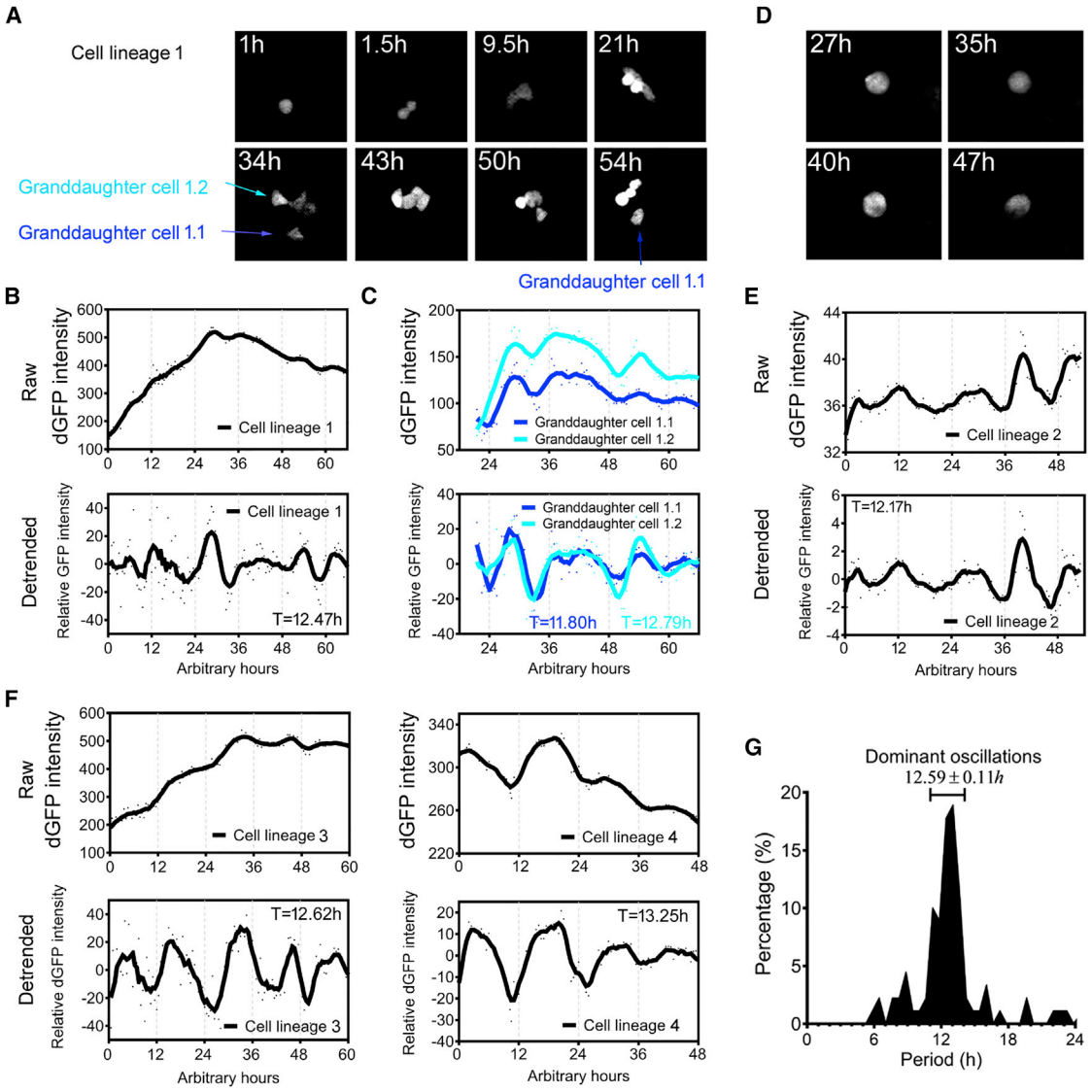

Figure 4. The Mammalian 12 hr Rhythm of Gene Expression Is Cell Autonomous

(A–F) *Eif2ak3*-dGFP cells were subjected to time-lapse imaging. Representative images (A and D) and quantifications of both raw and mathematically detrended data (B, C, E, and F).

(G) Distribution of the periods of dominant oscillations from 89 single-cell recordings.

Unlike the phases of 12 hr mRNA rhythms, the phases of 12 hr protein oscillations are distributed evenly throughout the diurnal cycle (Figures S5A and S6A). However, a closer examination reveals a clear phase separation of proteins involved in opposing metabolic pathways (Figure S6A). For instance, proteins participating in FAO, OXPHOS, and gluconeogenesis show peaks at early morning (ZT0∼ZT4) and early evening (ZT12∼ZT16) while proteins involved in glycolysis and fatty acid synthesis peak in the afternoon (ZT6∼ZT10) and late night (ZT18∼ZT22) (Figures 5B and 5C; Figure S6A). Purine de novo synthesis proteins peak at midday (ZT4∼ZT8) and midnight (ZT16∼ZT20), preceding the two peaks of 12 hr mRNA transcription at ZT12 and ZT24 (Figure S6A). These results demonstrated a prevalent 12 hr hepatic rhythms at the protein level.

XBP1s Transcriptionally Regulates the 12 hr Rhythm of Gene Expression

Systemic metabolism depends strongly on ER function and genetic ablation of UPR modulators severely impairs metabolic homeostasis (Bravo et al., 2013). Therefore, it is highly likely that the 12 hr rhythms of metabolic gene expression are in tune with the 12 hr oscillations of ER stress/UPR in vivo. Supporting this hypothesis, we found robust 12 hr oscillations of hepatic XBP1s and ATF4 (Figure 5D). Analysis of ribosome profiling data of ATF4 open reading frame usage (Janich et al., 2015) further confirmed the 12 hr oscillation of hepatic ATF4 translation in vivo (Figure 5E; Figure S5G). Moreover, we observed robust 12 hr rhythm of XBP1s expression in Tu-synchronized wild-type and *Bmal1* knockdown MEFs (Figures 5F and 5G), thus confirming

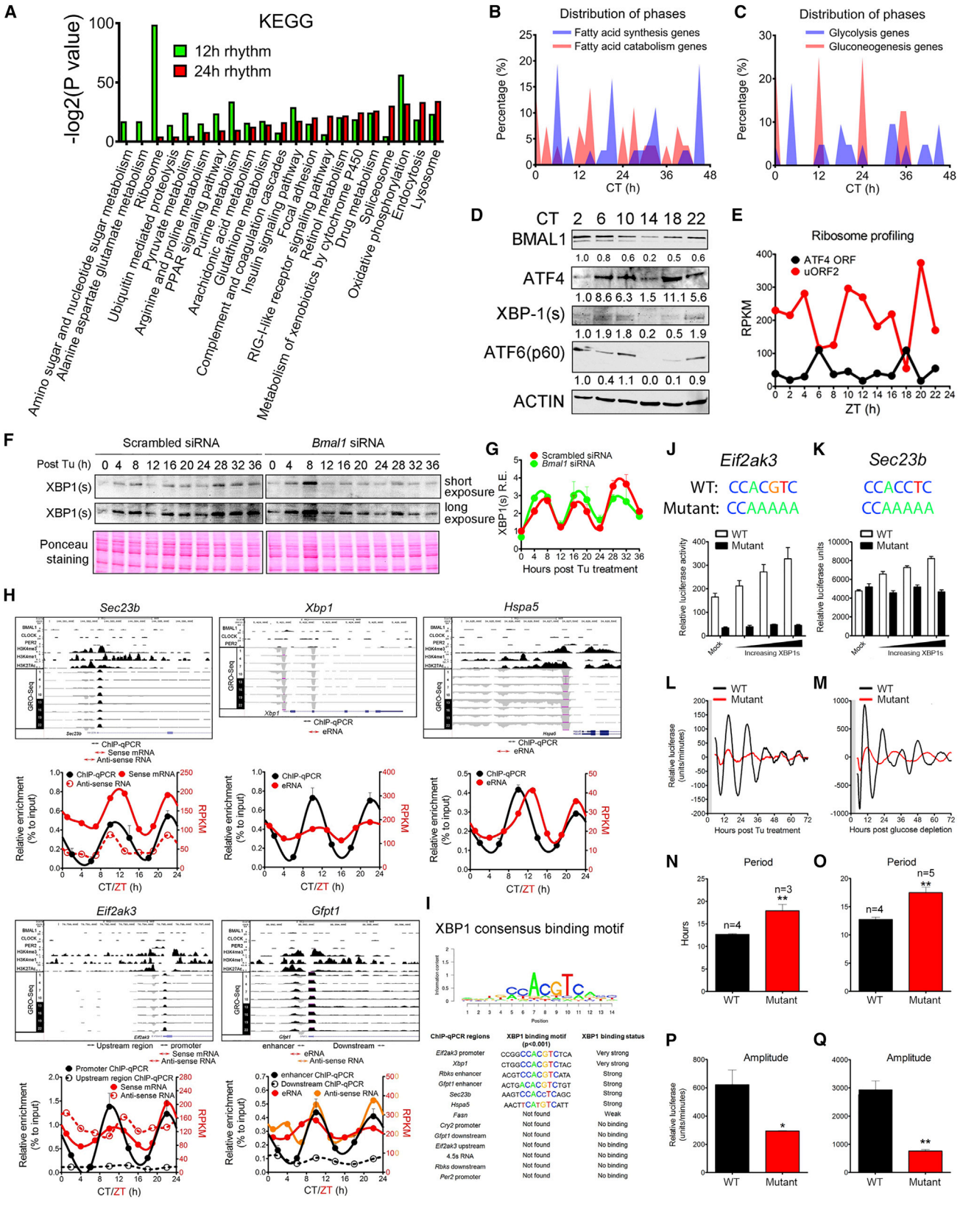

(legend on next page)

the cell autonomy and circadian clock independence of the 12 hr UPR.

We next hypothesized that XBP1s transcriptionally regulates the 12 hr rhythm of gene expression via direct chromatin recruitment to regulatory regions. To test this hypothesis, we first performed chromatin immunoprecipitation (ChIP)-qPCR on XBP1s in livers of mice housed under constant darkness conditions. We designed ten primer pairs targeting promoter (H3K4me3 high/H3K4me1 low), enhancer (H3K4me3 low/H3K4me1 high/eRNA positive), or negative control regions of seven genes exhibiting 12 hr rhythm of mRNA expression. In all cases, we detected robust 12 hr rhythm of XBP1s recruitment to either promoter or enhancer regions, with peak binding observed at CT10 and CT22 (Figure 5H; Figure S5H), consistent with its hepatic protein expression (Figure 5D). The 12 hr rhythm of XBP1s binding correlated with 12 hr rhythm of eRNA and pre-mRNA expression (Figure 5H; Figure S5H). Core circadian clock TF (BMAL1/CLOCK/PER2) binding sites are either absent or spatially separated from XBP1s binding sites (Figure 5H; Figure S5H), and no XBP1s recruitment was found on the promoter regions of core clock genes (Figure S5I). In addition, we found robust XBP1 binding motifs (CCACGTC) within 500 bp proximity (±250 bp) of the amplicon in six of seven genes with XBP1s binding (Figure 5I). Finally, we verified the cell-autonomous and *BMAL1*-independent 12 hr rhythms of XBP1s recruitment to *Sec23b*, *Eif2ak3*, and *Hspa5* gene regulatory regions in Tu-treated MEFs (Figures S5J–S5L). In sum, we demonstrate that a 12 hr rhythm of chromatin recruitment of XBP1s to 12 hr rhythm genes occurs in vivo and in vitro.

We next investigate whether XBP1s regulates 12 hr rhythm of gene expression. While XBP1s overexpression leads to a dose-dependent increase of both *Eif2ak3* and *Sec23b* promoter-driven luciferase activity, mutating the consensus XBP1s binding motif completely abolished this response (Figures 5J and 5K). Further, while stable *Eif2ak*3-dluc MEFs with WT promoter reveal robust 12 hr oscillation of luciferase activity in response to both Tu and GD treatments (Figures 3F–3H and 5L–5Q), mutating the XBP1s binding site significantly reduced the amplitude and lengthened the period (Figures 5L–5Q). Finally, small interfering RNA (siRNA)-mediated knockdown of XBP1 significantly dampened the 12 hr rhythm of metabolic and UPR gene expression and *Eif2ak3*-dluc oscillation in both Tu and GD-synchronized MEFs (Figures 3B, 3E, and 3F–3H; Figures S4G and S4H) yet failed to affect Dex-induced circadian oscillation of core clock genes (Figure S4I). Together, these results demonstrate that XBP1s transcriptionally regulates the 12 hr rhythm, but not the circadian rhythm, of gene expression.

12 hr Rhythm of Hepatic Metabolism Is Influenced by Feeding Behavior in Mice

A 12 hr rhythm of hepatic metabolic gene expression should impact the 12 hr rhythm of hepatic metabolite oscillation. To test this hypothesis, we performed a post hoc analysis of a published hepatic metabolomics dataset (Eckel-Mahan et al., 2013) and found ~15% (46 out 305) of the metabolites with a 12 hr period, including various fatty acids, 2-lyso-PCs, carnitine, sphingosine, 9-HODE, succinyl-CoA, ribose, and vitamin B1 (Figure 6A). The 12 hr rhythms of metabolites often correlate with the 12 hr oscillations of metabolic enzymes involved in the metabolism of these metabolites (Figure 6B; Figures S6B and S6C). Of particular interest are the 12 hr rhythms of *Lpcat3* expression and a number of 2-lyso-PCs. LPCAT3 functions to increase membrane fluidity by promoting the incorporation of polyunsaturated fatty acids into phospholipids (Figure 6B), and previous studies showed that *Lpcat3* induction significantly ameliorates ER stress through regulating ER membrane fluidity in mouse liver (Rong et al., 2013). These findings again indicate that the hepatic 12 hr clock can coordinate ER stress with metabolism to maintain systemic homeostasis.

Our findings raise the intriguing possibility that other peripheral tissues possess a 12 hr clock that perhaps helps to synchronize 12 hr metabolic homeostasis. To address this hypothesis, we measured the real-time respiratory exchange ratio (RER) of mice maintained under 12 hr/12 hr light/dark condition for 5 days and applied the eigenvalue/pencil method to these data. As expected, in addition to the circadian rhythm, oscillations with smaller periods were revealed in RER with ~12 hr rhythms exhibiting the second largest amplitude in all seven mice tested (Figures 6C–6E; Figures S6D–S6H). Daytime restricted feeding of mice from ZT3 to ZT11 significantly dampened the 12 hr rhythm of RER without altering their phases but had marginal effects on the amplitude of the circadian rhythm while altering their phases by ~6 hr (Figures 6C–6E; Figure S6H). These effects are not due to changed total food intake between

Figure 5. XBP1s Transcriptionally Regulates the Mammalian 12 hr Clock

(A) GO analysis of 12 hr and 24 hr cycling proteins.

(B and C) Distribution of phases for 12 hr cycling fatty acid (B) and glucose metabolism genes (C).

(D) Immunoblot of hepatic nuclear levels of UPR TFs and BMAL1 under CT conditions.

(E) Quantification of ribosome-binding intensity on hepatic ATF4 ORF or upstream open reading frame 2 (uORF2) by ribosome profiling at different zeitgeber times (ZTs).

(F and G) Representative immunoblot (F) and quantification from biological duplicates (G) of wild-type or *Bmal1* knockdown MEFs at different time points post-Tu treatment.

(H) Hepatic XBP1s binding to regulatory regions of key 12 hr genes under constant darkness conditions assayed by ChIP-qPCR (n = 3~4) overlaid with RPKM normalized quantification of mouse hepatic RNA synthesis rate under a 12 hr light/dark (L/D) schedule calculated from a published GRO-seq database (Fang et al., 2014) and BMAL1, CLOCK, PER2, H3K4me3, H3K4me1, and H3K27Ac cistromes (Koike et al., 2012). Amplicons of ChIP-qPCR and regions of RNA for quantification are illustrated by arrows of different colors.

(I) Consensus XBP1s binding motif and recovered motifs from XBP1s ChIP-qPCR amplicons.

(J and K) Transient luciferase assay using WT and XBP1s binding site mutant *Eif2ak3*-dluc (J) or *Sec23b*-dluc (K) vectors with increasing doses of XBP1s expression vector in MEFs (n = 4).

(L–Q) Real-time luminescence recording of WT and XBP1s binding site mutant stable *Eif2ak3*-dluc MEFs in response to Tu (L, N, and P) or glucose depletion (M, O, and Q). Quantified period (N and O) and amplitude (P and Q) were provided. Gray boxes indicate the duration of treatment. Data are graphed as the mean ± SEM. *$p < 0.05$, **$p < 0.01$.

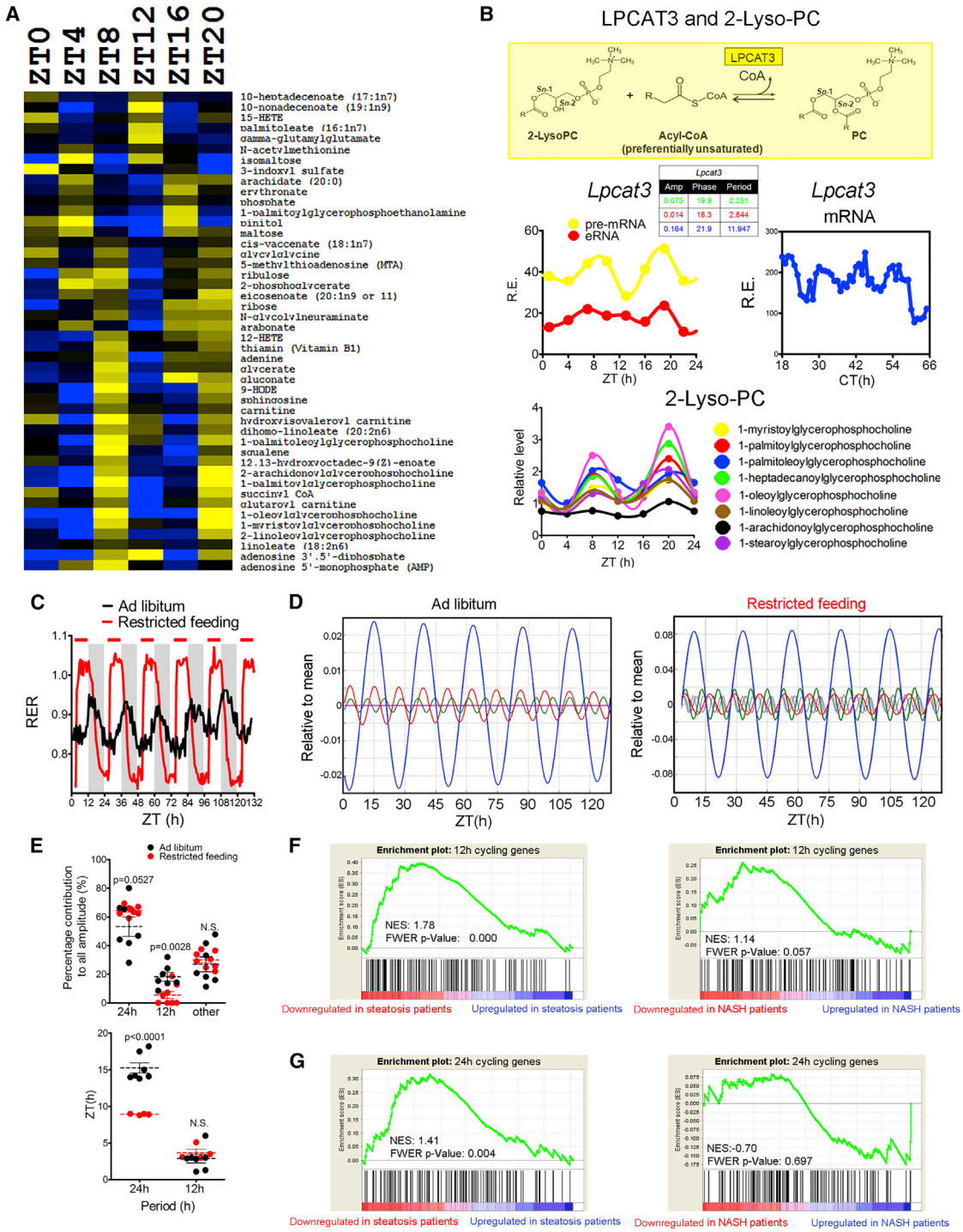

Figure 6. 12 hr Rhythm of Mouse Hepatic Metabolism

(A) Heatmap of mouse hepatic metabolites exhibiting 12 hr oscillation at different ZTs.

(B) 12 hr rhythm of *Lpcat3* mRNA expression is associated with 12 hr oscillations of various 2-Lyso-PC species in mouse liver. LPCAT3 catalyzes the conversion from 2-Lyso-PC to PC (top). Oscillations of *Lpcat3* pre-mRNA and eRNA transcription (Fang et al., 2014) (middle left), mature *Lpcat3* mRNA expression and its eigenvalue/pencil decomposition (middle right), and various 2-Lyso-PC levels (bottom).

(C–E) Averaged real-time RER values of mice housed under ad libitum or restricted feeding conditions. Time of food accessibility is indicated by red bars above the RER graph for the restricted feeding group (C). Eigenvalue/pencil deconvolutions of the average RER oscillations. Blue line: 24 hr oscillations; red line: 12 hr

(legend continued on next page)

normal and restricted feeding groups (Figures S6D–S6F). These data suggest that the feeding behavior-dependent 12 hr rhythm of systemic metabolism in mice is regulated differentially from the circadian rhythm.

The Downregulation of 12 hr Genes Is Associated with Human Progression to NAFLD

To determine whether the 12 hr clock also is influential in the maintenance of systemic metabolic homeostasis in humans, we examined the gene expression profiles of the 143 genes cycling with a 12 hr period at both the mRNA and the protein levels (Table S5) in human NAFLD patients (Ahrens et al., 2013) by performing gene set enrichment analysis (GSEA) (Subramanian et al., 2005). For comparison, we performed similar analyses using another cassette of 138 genes (Table S5) that exhibit circadian rhythms at both the mRNA and the protein levels. As shown in Figures 6F and 6G, the downregulation of 12 hr gene expression is strongly associated with progression to steatosis and modestly associated with non-alcoholic steatohepatitis (NASH). By contrast, the downregulation of circadian gene expression is less strongly associated with progression to steatosis, and no association was found between circadian gene expression changes and NASH. Since the 12 hr genes are functionally distinct from the circadian genes (Figures 1I and 1J), these results demonstrate that while independent from the circadian clock, the 12 hr clock likely plays an essential role in the maintenance of hepatic metabolic homeostasis in humans.

The 12 hr Rhythm of mtDNA Transcription Is Evolutionarily Conserved in Crustaceans and Mammals

The prevalent mammalian 12 hr rhythm of gene expression and metabolism is reminiscent of the 12 hr circatidal rhythms of coastal marine animals (Wilcockson and Zhang, 2008). Recently, establishment of the circatidal clock in the crustacean *E. pulchra* was reported to be independent from the circadian clock (Zhang et al., 2013). In light of the newly uncovered independence of the mammalian 12 hr clock from the circadian clock and the fact that mammals share common marine ancestors, we initially postulate that the mammalian 12 hr clock evolved from the ancient circatidal clock.

Intriguingly, previous work revealed robust 12 hr circatidal mRNA rhythms for ten mtDNA-encoded protein-coding genes (*Mt-Nd*1∼6, *Mt-Cox*1∼3, and *Cytb*) that encode for mitochondrial components of complexes I (NADH dehydrogenase) and IV (cytochrome *c* oxidase) in *E. pulchra* under free-running conditions (O'Neill et al., 2015). To test whether these 12 hr rhythms also are conserved in mammals, we performed a post hoc analysis of two published GRO-seq (Fang et al., 2014) and Nascent-seq datasets (Menet et al., 2012) that measured diurnal oscillations of mouse hepatic nascent RNA transcription. We observed robust global 12 hr rhythms of mtDNA-encoded RNA transcription from both strands of mtDNA in both datasets, with peak transcription occurring at ZT7∼ZT8 and ZT19∼ZT20, and nadir at ZT10∼ZT12 and ZT22∼ZT24 (Figure 7A; Figure S7A). In addition to nascent RNA transcription, both mtDNA-encoded mature mRNAs and proteins reveal robust 12 hr rhythms (Figures S7B and S7C and S5C–S5E; Table S5). Further, nuclear-encoded subunits of electron transport chain complexes also reveal strong 12 hr rhythms at the protein level (Figure S5C; Table S5). Collectively, these data indicate a coordinated 12 hr rhythm of OXPHOS gene transcription and translation between the nucleus and mitochondria. We further found 12 hr rhythm of mRNA expression in mitochondrial transcription factors B1 and B2 (*Tfb1m* and *Tfb2m*) (Figure S7D). In addition to functioning as a transcription factor regulating mtDNA transcription, TFB1M also is implicated in mitochondrial protein translation (Metodiev et al., 2009). Therefore, the 12 hr rhythms of nuclear-encoded *Tfb1m* and *Tfb2m* gene expression is likely responsible for the 12 hr rhythm of transcription and translation of mtDNA-encoded genes.

Finally, we confirmed the cell-autonomous 12 hr oscillation of *Mt-Nd1*, *mt-Nd2*, and *Mt-Atp6* gene expression in GD-synchronized MEFs, which are also independent of *Bmal1* (Figure 7B). On a final note, the calculated period value of 12.59 hr for the mammalian cell-autonomous *Eif2ak3* oscillation is close to the reported 12.7 hr circatidal period in free-running *E. pulchra* after tidal cues entrainment (Zhang et al., 2013). These findings are striking as they indicate that the circatidal rhythm of mtDNA-encoded gene transcription in marine animals is evolutionarily conserved in mammals, thereby supporting our hypothesis that the mammalian 12 hr clock perhaps evolved from the circatidal clock.

The 12 hr Rhythm of CREMA Is Evolutionarily Conserved in Both Nematodes and Mammals

Since the ER-related gene expression profiles were not reported in *E. pulchra*, it remains unclear whether the ER branch of 12 hr CREMA also is conserved evolutionarily in multiple species of lower organisms. To address this question, we examined a published microarray database in free-running *C. elegans* entrained by warm/cold temperature cycles (van der Linden et al., 2010). First, we confirmed the 12 hr rhythm of mtDNA-encoded OXPHOS gene transcription in nematodes (Figure 7C). Intriguingly, we further observed robust 12 hr mRNA rhythm of genes involved in ER stress and metabolism pathways (genes in Table S2). In fact, of all 70 genes that have orthologs in *C. elegans*, 43 (61%) of them show robust 12 hr cycling under both temperature entrainment as well as free-running conditions (Figure 7D; Figure S7E). These genes include *C. elegans* orthologs of *Xbp1*, *Hspa1a*, *Eif2ak3*, *Sec23b*, *Fasn*, *Pfkfb3*, and *P4ha1*, all of which have robust 12 hr rhythms in mouse liver (Table S2). The conservation of 12 hr rhythm in *C. elegans* is not limited to these core 12 hr cycling genes. In fact, of the top ten most robust mammalian 12 hr cycling genes, seven of their *C. elegans* orthologs also reveal robust 12 hr rhythms (Figures S7F and S7G). Since adult *C. elegans* has a fixed cell number of ∼1,000, the robust 12 hr oscillations of these genes suggest that 12 hr clock exists in most, if not all, cells in *C. elegans*.

oscillations; green line: 8 hr oscillations (D). The percentage contributions to the total amplitudes of RER oscillation from identified 24 hr, 12 hr, and the combined other oscillations (top) and the phases of identified 24 hr and 12 hr oscillation (bottom) in each individual mouse (E).

(F and G) GSEA analysis on 12 hr (F) or 24 hr (G) cycling genes compared with human hepatic steatosis (left) and NASH (right) microarray datasets. Normalized enrichment scores (NES) and FWER p values are shown for each analysis.

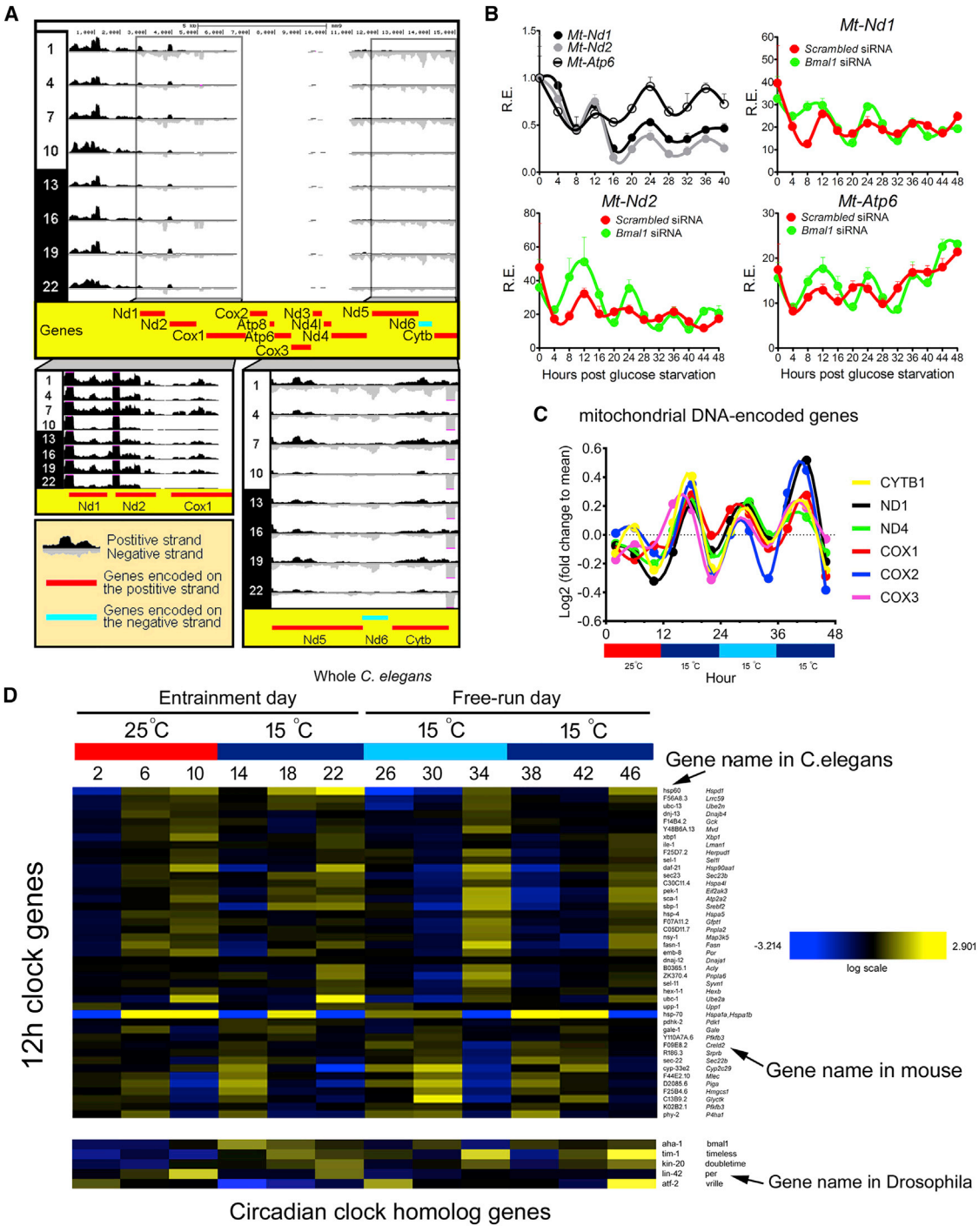

Figure 7. 12 hr CREMA Is Evolutionarily Conserved

(A) RPKM normalized quantification of mouse hepatic mtDNA-encoded RNA synthesis rate under a 12 hr L/D schedule calculated from published GRO-seq. UCSC Genome Browser snapshot of GRO-seq tracks across the 16.1 kb mouse mitochondrial genome. Protein-coding genes encoded on the positive strand are shown in red while genes on the negative strand are shown in blue. Boxes show UCSC tracks with higher magnification for specific regions.

(B) MEFs were transfected with different siRNA and glucose starved, and qPCR was performed post-GD (n = 3). Data are graphed as the mean ± SEM.

(C and D) *C. elegans* are entrained under 12 hr warm temperature (25°C)/12 hr cold temperature (15°C) for 4 days before being released into constant cold (15°C) condition for 24 hr, and mRNA from whole organisms were extracted and subjected to microarray analysis at 4 hr intervals. 12 hr cycling of mitochondrial DNA-encoded oxidative phosphorylation genes is shown in (C). Heatmap of 12 hr cycling ER stress and metabolism genes, as well as the lack of circadian oscillation of 24 hr clock genes, with *C. elegans* as well as mammalian/*Drosophila* ortholog gene names, are shown on the right (D).

More importantly, while the 12 hr rhythms are conserved in *C. elegans*, homologs of *Drosophila* and mammalian core circadian clock, as well as top 24 hr cycling mouse hepatic genes, do not exhibit circadian rhythms under the same conditions (Figure 7D; Figures S7H and S7I). The lack of circadian oscillation of canonical circadian clock genes in *C. elegans* has been previously reported in several studies, and these genes are believed to play roles in development rather than regulating circadian rhythms in nematodes (Romanowski et al., 2014; van der Linden et al., 2010). Given that the 12 hr clock is conserved, but not the 24 hr circadian clock, between nematodes and mammals, this observation strongly supports our hypothesis that the 12 hr clock evolved "separately" from the circadian clock and that the mammalian 12 hr clock is independent from the circadian clock.

DISCUSSION

Biological Rhythms Are Part of 'musica universalis'

In this study, we used a novel mathematical method to uncover all superimposed oscillations. Most of the current methodologies require the user to define a narrow period range and then use respective algorithms to find the optimal period within that range that minimizes the p value (Refinetti et al., 2007). These approaches are heavily biased since they presume that biological oscillations are pure rhythms with a single period. However, pure oscillation with a single frequency rarely exists in nature. Rather, physical rhythms often present as superpositions of basic waves such as the harmonic resonances found in music, light, and planetary motion. Our eigenvalue/pencil method, on the other hand, does not pre-assign a period and thus permits the identification of all superimposed oscillations in an unbiased manner. Using this method, we uncovered that, just like other forms of physical oscillations, biological oscillations also are composite rhythms consisting of oscillations of various frequencies. Interestingly, these oscillations often cycle at the harmonic of the circadian rhythm, presumably to ensure that most cellular oscillations are always in sync. Therefore, it appears that harmonic resonance is a common "universal" theme, a concept that was first proposed by Pythagoras as "musica universalis" over 2,000 years ago (Taruskin, 2008). According to this theory, all naturally appearing rhythms are in essence tuned to the rhythmic movements of celestial bodies (Taruskin, 2008). While the circadian rhythm is synchronized to the 24 hr light/dark cycle coinciding with the Earth's rotation, our findings suggest that the 12 hr clock may have evolved from the ancient circatidal clock, which is in turn entrained by the 12 hr tidal cues orchestrated mainly by the Moon.

The Cell Autonomy and Independence of the Mammalian 12 hr Clock

The relationship of 12 hr circatidal rhythms to 24 hr circadian rhythms remains elusive. A previous study reported that 12 hr rhythm of hepatic XBP1s and a few UPR genes is under the combined regulation of the circadian clock and fasting-feeding cues and therefore is not cell autonomous (Cretenet et al., 2010). However, our real-time luminescence and time-lapse microscopy experiments strongly support the existence of a cell-autonomous mammalian 12 hr clock. In single-cell microscopy experiment, we did observe variability of baseline GFP levels in individual *Eif2ak3*-dGFP recordings, which largely can be attributed to the fact that *Eif2ak3* is a key sensor of ER and metabolic stress and is thus very sensitive to the subtle changes of stress in each individual cell. Since the cells are not synchronized, the metabolic rate, cell cycle phase, and cell population density of/surrounding each individual cell can vary, and these factors can affect the temporal baseline changes of the *Eif2ak3*-dGFP reporter, leading to a more "noisy" raw data. However, after rigorous and unbiased mathematical detrending and eigenvalue/pencil decomposition, we unambiguously uncovered ~12 hr rhythm in ~90% of single-cell recordings. Moreover, as pointed above, even the single cell *Eif2ak3*-dGFP oscillations are not pure oscillations, but rather superimposed oscillations with dominant periods of ~12 hr and subperiods of ~8 hr and ~6 hr. Nevertheless, future studies are needed to determine whether cell-autonomous 12 hr rhythm also exists in other genes and cell lines.

Our study indicates that the cell-autonomous mammalian 12 hr rhythm is regulated independently from the circadian clock. Our finding also agrees with the recently identified independent circatidal clock in *E. pulchra*. Our reported conservation of 12 hr, but not circadian, genes between *C. elegans* and mouse implies that while the circadian clock machinery diverged early in evolution, the 12 hr clock machinery remained essentially unchanged even in species as divergent as nematodes and mammals. With that said, it is important to note that we are not ruling out the possibility that the 12 hr rhythms of some genes may be influenced by the circadian clock and/or the effects of similar external cues. Furthermore, while our data indicate that the 12 hr clock is independent from the circadian clock at the cellular level, they appear to be able to cross-talk at the systemic level (Hughes et al., 2012). Therefore, future studies are needed to investigate the physiological conditions by which these distinct clocks can interact systemically in multiple model organisms.

12 hr CREMA

Proteins exhibiting 12 hr rhythms of expression are prominently localized in both ER and mitochondria (Figure S6A), implying the coordination of these two organelles in the orchestration of 12 hr rhythms. This hypothesis is further supported by our data demonstrating that a 2 hr GD is sufficient to establish the 12 hr rhythms of genes involved in both UPR (*Eif2ak3*) and mitochondria-regulated metabolism (*Mt-Nd1* and *Mt-Nd2*). This observation is unsurprising, as in addition to active participation of both ER and mitochondria in extensive cellular metabolism, reciprocal functional dependence of these organelles has been comprehensively demonstrated (Kornmann, 2013). The ER-mitochondria interdependence is mainly mediated via regions of the ER that are physically associated with mitochondria, termed mitochondria-associated ER membranes (MAMs). Genes encoding proteins highly enriched on the MAMs, including *Ero1α*, *Pdia3*, and *Calnexin* (Simmen et al., 2010), all exhibited a 12 hr rhythmicity of gene expression. While it remains unclear whether the physical association of the ER and mitochondria is merely a consequence or plays a causal role in the regulation of the mammalian 12 hr clock, our results nonetheless

suggest that 12 hr CREMA are important for the maintenance of systemic metabolic homeostasis.

STAR★METHODS

Detailed methods are provided in the online version of this paper and include the following:

- KEY RESOURCES TABLE
- CONTACT FOR REAGENT AND RESOURCE SHARING
- EXPERIMENTAL MODEL AND SUBJECT DETAILS
  - Mice
  - Cell Lines
  - Synchronization of MEFs
- METHOD DETAILS
  - Eigenvalue/Pencil Method
  - siRNA Transient Transfections
  - Immunoblot
  - qRT-PCR
  - ChIP-qPCR
  - Cloning
  - Transient Luciferase Assay
  - Generation of Stable MEFs Lines
  - Real-Time Luminescence Assay
  - Time-Lapse Microscopy
  - Measurement of Plasma Glucose and Insulin
  - Metabolic Profiling Using CLAMS
- QUANTIFICATION AND STATISTICAL ANALYSIS
  - Data Analysis by ARSER, RAIN and JTK_CYCLE
  - Gene Ontology Analysis
  - Post Hoc Analysis of Hepatic SILAC Data
  - Post Hoc Analysis of Hepatic Metabolomic Data
  - Post Hoc Analysis of C. elegans Microarray
  - Gene Set Enrichment Analysis
  - Statistical Analysis
- DATA AND SOFTWARE AVAILABILITY

SUPPLEMENTAL INFORMATION

Supplemental Information includes seven figures, six tables, and one movie and can be found with this article online at http://dx.doi.org/10.1016/j.cmet.2017.05.004.

AUTHOR CONTRIBUTIONS

B.Z. and A.C.A. designed research; C.C.D. and B.W.O. supervised the project; B.Z. performed experiments; Q.Z. and A.C.A. performed mathematical analyses; B.Z. analyzed data; E.M.M. assisted in the time-lapse microscope experiment; Y.P. generated the *Eif2ak3*-dGFP cell line; and B.Z., Q.Z., B.Y., A.C.A., C.C.D., and B.W.O. wrote the paper.

ACKNOWLEDGMENTS

We greatly thank Naomi Gonzalez at BCM for technical support and Dr. Xi Chen at BCM for suggestions and comments on XBP1-related research as well as providing the XBP1s overexpression construct. This research was supported by grants from the NIH (U24 DK097748 and R01 HD07857 to B.W.O.) and by the Brockman Medical Research Foundation to B.W.O. and C.C.D. In addition, this research also was supported by grants from the Center for Advancement of Science in Space, Peter J. Fluor Family Fund, Philip J. Carroll, Jr., Professorship, and Joyce Family Foundation to C.C.D. and NSF Grant CCF-1320866, as well as DFG (German Science Foundation) Grant AN-693/1-1, to A.C.A.

Received: August 3, 2016
Revised: December 11, 2016
Accepted: May 18, 2017
Published: June 6, 2017

REFERENCES

Ahrens, M., Ammerpohl, O., von Schönfels, W., Kolarova, J., Bens, S., Itzel, T., Teufel, A., Herrmann, A., Brosch, M., Hinrichsen, H., et al. (2013). DNA methylation analysis in nonalcoholic fatty liver disease suggests distinct disease-specific and remodeling signatures after bariatric surgery. Cell Metab. *18*, 296–302.

Ayala, D.E., Hermida, R.C., Garcia, L., Iglesias, T., and Lodeiro, C. (1990). Multiple component analysis of plasma growth hormone in children with standard and short stature. Chronobiol. Int. *7*, 217–220.

Bjerner, B., Holm, A., and Swensson, A. (1955). Diurnal variation in mental performance; a study of three-shift workers. Br. J. Ind. Med. *12*, 103–110.

Bravo, R., Parra, V., Gatica, D., Rodriguez, A.E., Torrealba, N., Paredes, F., Wang, Z.V., Zorzano, A., Hill, J.A., Jaimovich, E., et al. (2013). Endoplasmic reticulum and the unfolded protein response: dynamics and metabolic integration. Int. Rev. Cell Mol. Biol. *301*, 215–290.

Broughton, R., and Mullington, J. (1992). Circasemidian sleep propensity and the phase-amplitude maintenance model of human sleep/wake regulation. J. Sleep Res. *1*, 93–98.

Carpenter, A.E., Jones, T.R., Lamprecht, M.R., Clarke, C., Kang, I.H., Friman, O., Guertin, D.A., Chang, J.H., Lindquist, R.A., Moffat, J., et al. (2006). CellProfiler: image analysis software for identifying and quantifying cell phenotypes. Genome Biol. *7*, R100.

Colquhoun, W.P., Paine, M.W., and Fort, A. (1978). Circadian rhythm of body temperature during prolonged undersea voyages. Aviat. Space Environ. Med. *49*, 671–678.

Cretenet, G., Le Clech, M., and Gachon, F. (2010). Circadian clock-coordinated 12 Hr period rhythmic activation of the IRE1alpha pathway controls lipid metabolism in mouse liver. Cell Metab. *11*, 47–57.

Eckel-Mahan, K.L., Patel, V.R., de Mateo, S., Orozco-Solis, R., Ceglia, N.J., Sahar, S., Dilag-Penilla, S.A., Dyar, K.A., Baldi, P., and Sassone-Corsi, P. (2013). Reprogramming of the circadian clock by nutritional challenge. Cell *155*, 1464–1478.

Fang, B., Everett, L.J., Jager, J., Briggs, E., Armour, S.M., Feng, D., Roy, A., Gerhart-Hines, Z., Sun, Z., and Lazar, M.A. (2014). Circadian enhancers coordinate multiple phases of rhythmic gene transcription in vivo. Cell *159*, 1140–1152.

Haus, E., Dumitriu, L., Nicolau, G.Y., Bologa, S., and Sackett-Lundeen, L. (2001). Circadian rhythms of basic fibroblast growth factor (bFGF), epidermal growth factor (EGF), insulin-like growth factor-1 (IGF-1), insulin-like growth factor binding protein-3 (IGFBP-3), cortisol, and melatonin in women with breast cancer. Chronobiol. Int. *18*, 709–727.

Hoogerwerf, W.A., Sinha, M., Conesa, A., Luxon, B.A., Shahinian, V.B., Cornélissen, G., Halberg, F., Bostwick, J., Timm, J., and Cassone, V.M. (2008). Transcriptional profiling of mRNA expression in the mouse distal colon. Gastroenterology *135*, 2019–2029.

Huang, d.W., Sherman, B.T., and Lempicki, R.A. (2009). Systematic and integrative analysis of large gene lists using DAVID bioinformatics resources. Nat. Protoc. *4*, 44–57.

Hughes, M.E., DiTacchio, L., Hayes, K.R., Vollmers, C., Pulivarthy, S., Baggs, J.E., Panda, S., and Hogenesch, J.B. (2009). Harmonics of circadian gene transcription in mammals. PLoS Genet. *5*, e1000442.

Hughes, M.E., Hogenesch, J.B., and Kornacker, K. (2010). JTK_CYCLE: an efficient nonparametric algorithm for detecting rhythmic components in genome-scale data sets. J. Biol. Rhythms *25*, 372–380.

Hughes, M.E., Hong, H.K., Chong, J.L., Indacochea, A.A., Lee, S.S., Han, M., Takahashi, J.S., and Hogenesch, J.B. (2012). Brain-specific rescue of Clock reveals system-driven transcriptional rhythms in peripheral tissue. PLoS Genet. *8*, e1002835.

Ionita, A.C., and Antoulas, A.C. (2013). Parametrized reduction using reduced-basis and the Loewner framework. In Reduced Order Methods for Modeling and Computational Reduction, A. Quarteroni and G. Rozza, eds. (Springer), pp. 51–66.

Ionita, A.C., and Antoulas, A.C. (2014). Data-driven parametrized model reduction in the Loewner framework. SIAM J. Sci. Comput. *36*, A984–A1007.

Janich, P., Arpat, A.B., Castelo-Szekely, V., Lopes, M., and Gatfield, D. (2015). Ribosome profiling reveals the rhythmic liver translatome and circadian clock regulation by upstream open reading frames. Genome Res. *25*, 1848–1859.

Keller, M., Mazuch, J., Abraham, U., Eom, G.D., Herzog, E.D., Volk, H.D., Kramer, A., and Maier, B. (2009). A circadian clock in macrophages controls inflammatory immune responses. Proc. Natl. Acad. Sci. USA *106*, 21407–21412.

Koike, N., Yoo, S.H., Huang, H.C., Kumar, V., Lee, C., Kim, T.K., and Takahashi, J.S. (2012). Transcriptional architecture and chromatin landscape of the core circadian clock in mammals. Science *338*, 349–354.

Kornmann, B. (2013). The molecular hug between the ER and the mitochondria. Curr. Opin. Cell Biol. *25*, 443–448.

Menet, J.S., Rodriguez, J., Abruzzi, K.C., and Rosbash, M. (2012). Nascent-Seq reveals novel features of mouse circadian transcriptional regulation. eLife *1*, e00011.

Metodiev, M.D., Lesko, N., Park, C.B., Cámara, Y., Shi, Y., Wibom, R., Hultenby, K., Gustafsson, C.M., and Larsson, N.G. (2009). Methylation of 12S rRNA is necessary for in vivo stability of the small subunit of the mammalian mitochondrial ribosome. Cell Metab. *9*, 386–397.

Miller, B.H., McDearmon, E.L., Panda, S., Hayes, K.R., Zhang, J., Andrews, J.L., Antoch, M.P., Walker, J.R., Esser, K.A., Hogenesch, J.B., and Takahashi, J.S. (2007). Circadian and CLOCK-controlled regulation of the mouse transcriptome and cell proliferation. Proc. Natl. Acad. Sci. USA *104*, 3342–3347.

O'Neill, J.S., Lee, K.D., Zhang, L., Feeney, K., Webster, S.G., Blades, M.J., Kyriacou, C.P., Hastings, M.H., and Wilcockson, D.C. (2015). Metabolic molecular markers of the tidal clock in the marine crustacean Eurydice pulchra. Curr. Biol. *25*, R326–R327.

Otsuka, K., Cornélissen, G., and Halberg, F. (1997). Circadian rhythmic fractal scaling of heart rate variability in health and coronary artery disease. Clin. Cardiol. *20*, 631–638.

Refinetti, R., Lissen, G.C., and Halberg, F. (2007). Procedures for numerical analysis of circadian rhythms. Biol. Rhythm Res. *38*, 275–325.

Robles, M.S., Cox, J., and Mann, M. (2014). In vivo quantitative proteomics reveals a key contribution of post-transcriptional mechanisms to the circadian regulation of liver metabolism. PLoS Genet. *10*, e1004047.

Romanowski, A., Garavaglia, M.J., Goya, M.E., Ghiringhelli, P.D., and Golombek, D.A. (2014). Potential conservation of circadian clock proteins in the phylum Nematoda as revealed by bioinformatic searches. PLoS ONE *9*, e112871.

Rong, X., Albert, C.J., Hong, C., Duerr, M.A., Chamberlain, B.T., Tarling, E.J., Ito, A., Gao, J., Wang, B., Edwards, P.A., et al. (2013). LXRs regulate ER stress and inflammation through dynamic modulation of membrane phospholipid composition. Cell Metab. *18*, 685–697.

Simmen, T., Lynes, E.M., Gesson, K., and Thomas, G. (2010). Oxidative protein folding in the endoplasmic reticulum: tight links to the mitochondria-associated membrane (MAM). Biochim. Biophys. Acta *1798*, 1465–1473.

Stashi, E., Lanz, R.B., Mao, J., Michailidis, G., Zhu, B., Kettner, N.M., Putluri, N., Reineke, E.L., Reineke, L.C., Dasgupta, S., et al. (2014). SRC-2 is an essential coactivator for orchestrating metabolism and circadian rhythm. Cell Rep. *6*, 633–645.

Subramanian, A., Tamayo, P., Mootha, V.K., Mukherjee, S., Ebert, B.L., Gillette, M.A., Paulovich, A., Pomeroy, S.L., Golub, T.R., Lander, E.S., and Mesirov, J.P. (2005). Gene set enrichment analysis: a knowledge-based approach for interpreting genome-wide expression profiles. Proc. Natl. Acad. Sci. USA *102*, 15545–15550.

Taruskin, R. (2008). Music in the western world: a history in documents, second edition. Choral Journal *48*, 68–70.

Thaben, P.F., and Westermark, P.O. (2014). Detecting rhythms in time series with RAIN. J. Biol. Rhythms *29*, 391–400.

van der Linden, A.M., Beverly, M., Kadener, S., Rodriguez, J., Wasserman, S., Rosbash, M., and Sengupta, P. (2010). Genome-wide analysis of light- and temperature-entrained circadian transcripts in Caenorhabditis elegans. PLoS Biol. *8*, e1000503.

Wang, X., Eno, C.O., Altman, B.J., Zhu, Y., Zhao, G., Olberding, K.E., Rathmell, J.C., and Li, C. (2011). ER stress modulates cellular metabolism. Biochem. J. *435*, 285–296.

Westermark, P.O., and Herzel, H. (2013). Mechanism for 12 hr rhythm generation by the circadian clock. Cell Rep. *3*, 1228–1238.

Wilcockson, D., and Zhang, L. (2008). Circatidal clocks. Curr. Biol. *18*, R753–R755.

Xu, C., Bailly-Maitre, B., and Reed, J.C. (2005). Endoplasmic reticulum stress: cell life and death decisions. J. Clin. Invest. *115*, 2656–2664.

Yang, R., and Su, Z. (2010). Analyzing circadian expression data by harmonic regression based on autoregressive spectral estimation. Bioinformatics *26*, i168–i174.

Yang, G., Chen, L., Grant, G.R., Paschos, G., Song, W.L., Musiek, E.S., Lee, V., McLoughlin, S.C., Grosser, T., Cotsarelis, G., and FitzGerald, G.A. (2016). Timing of expression of the core clock gene Bmal1 influences its effects on aging and survival. Sci. Transl. Med. *8*, 324ra16.

Zhang, L., Hastings, M.H., Green, E.W., Tauber, E., Sladek, M., Webster, S.G., Kyriacou, C.P., and Wilcockson, D.C. (2013). Dissociation of circadian and circatidal timekeeping in the marine crustacean Eurydice pulchra. Curr. Biol. *23*, 1863–1873.

Zhang, R., Lahens, N.F., Ballance, H.I., Hughes, M.E., and Hogenesch, J.B. (2014). A circadian gene expression atlas in mammals: implications for biology and medicine. Proc. Natl. Acad. Sci. USA *111*, 16219–16224.

Zhu, B., Gates, L.A., Stashi, E., Dasgupta, S., Gonzales, N., Dean, A., Dacso, C.C., York, B., and O'Malley, B.W. (2015). Coactivator-dependent oscillation of chromatin accessibility dictates circadian gene amplitude via REV-ERB loading. Mol. Cell *60*, 769–783.

STAR★METHODS

KEY RESOURCES TABLE

REAGENT or RESOURCE	SOURCE	IDENTIFIER
Antibodies		
Rabbit polyclonal anti-ACC1	Cell Signaling Technology	Cat# 4190S, RRID: AB_10547752
Rabbit monoclonal anti-FASN	Cell Signaling Technology	Cat# 3180S, RRID: AB_2100796
Rabbit anti-beta-Actin Monoclonal Antibody, HRP Conjugated, Clone 13E5	Cell Signaling Technology	Cat# 5125, RRID: AB_1903890
Rabbit monoclonal anti-ATF4	Cell Signaling Technology	Cat# 11815S, RRID: AB_2616025
Rabbit monoclonal anti-HSP40	Cell Signaling Technology	Cat# 4871S, RRID: AB_2094571
Rabbit monoclonal anti-HSP90	Cell Signaling Technology	Cat# 4877S, RRID: AB_2233307
Rabbit monoclonal anti-HSP60	Cell Signaling Technology	Cat# 12165, RRID: AB_2636980
Rabbit polyclonal anti-BMAL1	Abcam	Cat# ab3350, RRID: AB_303729
Rabbit monoclonal [EPR13466(2)] to MT-ND1	Abcam	Cat# ab181848
Rabbit polyclonal anti-ACLY	Bethyl Laboratories	Cat# A303-866A, RRID: AB_2620217
Rabbit polyclonal anti-XBP1	Santa Cruz Biotechnology	Cat# sc-7160, RRID: AB_794171
Rabbit polyclonal anti-GCK	Santa Cruz Biotechnology	Cat# sc-7908, RRID: AB_2107620
Rabbit polyclonal anti-ATF6-α	Santa Cruz Biotechnology	Cat# sc-22799, RRID: AB_2242950
Rabbit polyclonal anti-XBP1s	BioLegend	Cat# 619501, RRID: AB_315907
Bacterial and Virus Strains		
Eif2ak3 promoter-pGreenfire-mCMV-dscGFP-EF1-Puro lentivirus	This paper	N/A
Chemicals, Peptides, and Recombinant Proteins		
Tunicamycin	EMD Millipore	Cat# 654380
2-Deoxy-D-glucose	EMD Millipore	Cat# 25972
Dexamethasone $\geq$ 98% (HPLC)	Sigma	Cat# D1756
Polybrene	Santa Cruz Biotechnology	Cat# sc-134220
Hygromycin B	Thermo Fisher Scientific	Cat# 10687010
Lipofectamine 2000 Transfection Reagent	Thermo Fisher Scientific	Cat# 11668027
Lipofectamine RNAiMAX Transfection Reagent	Thermo Fisher Scientific	Cat# 13778030
HEPES	Thermo Fisher Scientific	Cat# 15630080
SuperScript VILO Master Mix	Thermo Fisher Scientific	Cat# 11755050
Micrococcal Nuclease	New England Biolabs	Cat# M0247S
Sodium Pyruvate	Thermo Fisher Scientific	Cat# 11360070
PEG-it Virus Precipitation Solution	System Biosciences	Cat# LV810A-1
RNase A, DNase and protease-free	Thermo Fisher Scientific	Cat# EN0531
TaqMan Universal Master Mix II, no UNG	Thermo Fisher Scientific	Cat# 4440047
Power SYBR Green Master Mix	Thermo Fisher Scientific	Cat# 4367660
Dialyzed Fetal Bovine Serum	Thermo Fisher Scientific	Cat# 26400036
Fetal Bovine Serum	Thermo Fisher Scientific	Cat# 10437028
D-glucose	Sigma	Cat# G8270
Sodium Acetate	Sigma	Cat# S2889
2-Mercaptoethanol	Sigma	Cat# M3148
DMSO	Sigma	Cat# D8418
NP-40	Sigma	Cat# N3516
Sodium chloride	Sigma	Cat# S7653
Tris/glycine/SDS buffer	Bio-Rad	Cat# 161-0772

(*Continued on next page*)

Continued

REAGENT or RESOURCE	SOURCE	IDENTIFIER
TBST	Cell Signaling Technology	Cat# 9997
10% SDS	GIBCO	Cat# 15553-035
Triton X-100	Promega	Cat# H5142
Tween 20	Fisher Scientific	Cat# BP337-100
BSA	Sigma	Cat# A9647
EDTA	Cell Signaling Technology	Cat# 7011S
Nonfat dry milk	Bio-Rad	Cat# 170-6404
BCA Protein Assay Reagent A	Thermo Fisher Scientific	Cat# 23223
BCA Protein Assay Reagent B	Thermo Fisher Scientific	Cat# 23224
iBlot Gel transfer stacks Nitrocellulose	Life Technologies	Cat# IB301001
Sodium deoxycholate	Sigma	Cat# D6750
Mouse Genomic DNA	Promega	Cat# G3091
Ponceau S solution	Sigma	Cat# P7170
VivoGlo Luciferin, In Vivo Grade	Promega	Cat# P1041
Restore western blot stripping buffer	Thermo Fisher Scientific	Cat# 21063
Penicillin Streptomycin	Thermo Fisher Scientific	Cat# 15070063
Pellet Paint Co-Precipitant	EMD Millipore	Cat# 69049
Q5 High-Fidelity DNA Polymerase	New England Biolabs	Cat# M0491S
Criterion pre-cast gradient SDS-PAGE gel (4%-20%)	Bio-Rad	Cat# 5671094
TaKaRa Ex Taq DNA Polymerase	Clontech	Cat# RR001A
T4 DNA Ligase	New England Biolabs	Cat# M0202
Antarctic Phosphatase	New England Biolabs	Cat# M0289S
Ethanol 200 proof	Decon Labs	Cat# 2701
Isopropanol	Sigma	Cat# I9516
cOmplete Protease Inhibitor Cocktail	Roche	Cat# 11697498001
PhosSTOP	Roche	Cat# 4906845001
DMEM, high glucose	Thermo Fisher Scientific	Cat# 11965092
DMEM, no glucose	Thermo Fisher Scientific	Cat# 11966025
Proteinase K	Thermo Fisher Scientific	Cat# AM2544
0.45μM syringe filter	Thermo Fisher Scientific	Cat# 09-740-106
SacI	New England Biolabs	Cat# R1056
SpeI	New England Biolabs	Cat# R1033
XhoI	New England Biolabs	Cat# R1046
ClaI	New England Biolabs	Cat# R0197
Puromycin Dihydrochloride	Thermo Fisher Scientific	Cat# A1113803
Critical Commercial Assays		
SimpleChIP Plus Enzymatic Chromatin IP Kit	Cell Signaling Technology	Cat# 9005S
PureLink RNA mini kit	Life Technologies	Cat# 12183025
Dual-luciferase Reporter assay system	Promega	Cat# E1960
Insulin ELISA kit	EMD Millipore	Cat# EZRMI-13K
Q5 Site-Directed Mutagenesis Kit	New England Biolabs	Cat# E0554S
One touch ultra glucose meter and strips	LifeScan	N/A
Experimental Models: Cell Lines		
293TN producer cell line	System Biosciences	Cat# LV900A-1
Immortalized mouse embryonic fibroblasts	Stashi et al., 2014	N/A

(*Continued on next page*)

Continued

REAGENT or RESOURCE	SOURCE	IDENTIFIER
Deposited Data		
Raw and processed single cell Eif2ak3-dGFP images	This paper	http://dx.doi.org/10.17632/wk8sfwbfw4.1
Experimental Models: Organisms/Strains		
Mouse: C57BL/6J male mice	The Jackson Laboratory	JAX:000664
Oligonucleotides		
Eif2ak3-dluc forward 5′- ATAGAGC TCAAACCAACCGGGAGACTTAAT-3′	Integrated DNA Technologies	Custom primer
Eif2ak3-dluc reverse 5′- ATACTCGA GCCAGCAGCAGGAACAGAA-3′	Integrated DNA Technologies	Custom primer
Eif2ak3-dGFP forward 5′- ATAATCGA TAAACCAACCGGGAGACTTAAT-3′	Integrated DNA Technologies	Custom primer
Eif2ak3-dGFP reverse 5′- ATAACTAG TCCAGCAGCAGGAACAGAA-3′	Integrated DNA Technologies	Custom primer
Sec23b-dluc forward 5′- ATAATCGA TAGCACAGAAACCACAGCA-3′	Integrated DNA Technologies	Custom primer
Sec23b-dluc reverse 5′- ATAACTA GTTTCACCATTGCAGAGCCA-3′	Integrated DNA Technologies	Custom primer
Eif2ak3-dluc mutant forward 5′- CAGT GGCTGAtttttGGCCGGGCAGCTC-3′	Integrated DNA Technologies	Custom primer
Eif2ak3-dluc mutant reverse 5′- CCA CCTGAGTGACAGCCT-3′	Integrated DNA Technologies	Custom primer
Sec23b-dluc mutant forward 5′- ACTG TGAGCTttttTGGACTTGGCGGTGG-3′	Integrated DNA Technologies	Custom primer
Sec23b-dluc mutant reverse 5′- CGA TTGGTCACCGCTCCG-3′	Integrated DNA Technologies	Custom primer
siRNA oligonucleotides	Dharmacon	Please see siRNA Transient Transfections section
Mouse ChIP-qPCR Primer Sequences	Integrated DNA Technologies	Please see Table S6
Mouse qRT-PCR Primer Sequences	Integrated DNA Technologies	Please see Table S6
Recombinant DNA		
XBP1s-pHAGE	A gift from Dr. Xi Chen at BCM	N/A
Eif2ak3-dluc	This paper	N/A
Eif2ak3-dluc mutant	This paper	N/A
Sec23b-dluc	This paper	N/A
Sec23b-dluc mutant	This paper	N/A
Eif2ak3-dGFP	This paper	N/A
pMD2.G	Unpublished and a gift from Didier Trono	Addgene Cat# 12259
psPAX2	Unpublished and a gift from Didier Trono	Addgene Cat# 12260
Software and Algorithms		
Eigenvalue/pencil	This paper	N/A
RAIN	Thaben and Westermark, 2014	http://www.bioconductor.org/packages/release/bioc/html/rain.html
JTK_CYCLE	Hughes et al., 2010	https://github.com/gangwug/MetaCycle
ARSER	Yang and Su, 2010	https://github.com/gangwug/MetaCycle
Bioconductor 3.4	N/A	https://www.bioconductor.org/news/bioc_3_4_release/
CircWaveBatch 3.3	EUCLOCK	https://www.euclock.org/results/item/circ-wave-batch.html
MATLAB R2017a	MathWorks	https://www.mathworks.com/products/new_products/latest_features.html

(*Continued on next page*)

Continued

REAGENT or RESOURCE	SOURCE	IDENTIFIER
GraphPad Prism 7	GraphPad Software	https://www.graphpad.com/scientific-software/prism/
ImageJ Software	NIH	https://imagej.nih.gov/ij/
Cell Profiler 2.20	Carpenter et al., 2006	http://cellprofiler.org/releases/
LumiCycle Analysis 2.54	ActiMetrics	http://actimetrics.com/downloads/lumicycle/
UCSC Genome Browser	UCSC	https://genome.ucsc.edu/cgi-bin/hgGateway
GSEA 2.0	The Broad Institute; Subramanian et al., 2005	http://software.broadinstitute.org/gsea/index.jsp
DAVID Bioinformatics Resources 6.8	NIH; Huang et al., 2009	https://david.ncifcrf.gov/
Screen Motif	Galaxy Cistrome/Integrative Analysis/Motif	http://cistrome.dfci.harvard.edu/ap/root
VirtualDubMod 1.5.10	Intel Software	https://sourceforge.net/projects/virtualdubmod/files/
Venn Diagram Plotter v.1.5.5228.29250	Department of Energy and PNNL	https://omics.pnl.gov/software/venn-diagram-plotter
Gene Cluster 3.0	Originally written by Michael Eisen at Stanford University	http://bonsai.hgc.jp/~mdehoon/software/cluster/software.htm#ctv
Java TreeView 3.0 alpha03	Open Source Software	https://bitbucket.org/TreeView3Dev/treeview3/
CLAMS data eXamination tool	Columbus Instruments	http://www.colinst.com/products/clams-hc-comprehensive-lab-animal-monitoring-system-for-home-cages#CLAX
Other		
NCBI Aceview (*AceView* offers a comprehensive annotation of human, mouse and nematode genes)	NIH	https://www.ncbi.nlm.nih.gov/IEB/Research/Acembly/index.html

CONTACT FOR REAGENT AND RESOURCE SHARING

Further information and requests for resources and reagents should be directed and will be fulfilled by the Lead Contact, Bert W. O'Malley (berto@bcm.edu).

EXPERIMENTAL MODEL AND SUBJECT DETAILS

Mice

For mice housed under constant darkness, a cohort of 8~12 weeks old male C57BL/6J mice were entrained under a normal 12 hr:12 hr light/dark conditions for at least two weeks before released into constant darkness. Following 36 hr of constant darkness, liver tissue and plasma was harvested at 2 hr intervals for a total of 48 hr (n = 3 at each CT). During all these time, the mice were fed ad libitum. For mice housed under 12 hr light/12 hr dark conditions, mice were entrained under a strict 12 hr light/12 hr dark schedule for two weeks before the experiment. After entrainment, one cohort of mice (n = 7) were fed ad libitum; while the second cohort of mice (n = 8) were restricted fed only during the 12 hr light period (ZT3 to ZT11). During these times, all the mice were still housed under the normal 12 hr light/12 hr dark schedule. The Baylor College of Medicine Institutional Animal Care and Utilization Committee approved all experiments.

Cell Lines

293TN producers were purchased from System biosciences and is a derivative of HEK293T cells that express a neomycin resistance marker. 293TN cells were cultured in DMEM (4.5g/L glucose) supplemented with 10% FBS at 37°C with 5% CO_2. The sex of this cell line was unknown.

Synchronization of MEFs

MEFs were isolated from male SRC-$2^{fl/fl}$ mice and immortalized by SV40 T antigen as previously described (Stashi et al., 2014). For tunicamycin treatment, MEFs were cultured in DMEM (4.5g/L glucose) supplemented with 10% FBS and treated with the indicated

concentration of tunicamycin for 2 hr, and then washed with 1X PBS before cultured in the same medium. For glucose depletion treatment, MEFs were cultured in DMEM (10mM glucose) supplemented with 10% dialyzed FBS and then treated with DMEM (no glucose) supplemented with 10% dialyzed FBS for 2 hr before replaced with DMEM (10mM glucose) supplemented with 10% dialyzed FBS. For 2-DG treatment, MEFs were cultured in DMEM (10mM glucose) supplemented with 10% dialyzed FBS and then treated with different concentration of 2-DG for 2 hr in DMEM (10mM glucose) supplemented with 10% dialyzed FBS before replaced with DMEM (10mM glucose) supplemented with 10% dialyzed FBS. For dexamethasone treatment, MEFs were cultured in DMEM (4.5g/L glucose) supplemented with 10% FBS and treated with 100nM Dex for 30mins, and then washed with 1X PBS before cultured in the same medium. For all cell culture experiments, cells were cultured at 37°C with 5% CO_2.

METHOD DETAILS

Eigenvalue/Pencil Method

Selecting Hepatic Genes for Analysis

We initially applied our approach to a high resolution hepatic gene expression microarray dataset from mice kept under constant darkness (analyzed at 1 hr interval for a total of 48 hr) (Hughes et al., 2009). This microarray dataset has the highest resolution available with this degree of granularity and therefore is uniquely suitable for robustly revealing oscillations of various periods. In this study, liver RNA samples from 3∼5 mice at each CT were pooled and analyzed using Affymetrix array. To select genes that are expressed in mouse liver for eigenvalue/pencil analysis, we first determined the background gene expression levels by randomly selecting 57 genes that are known to be not expressed in the liver. These genes include 45 keratin family members preferentially expressed in the skin, three probes for nestin gene preferentially expressed in the neurons and 9 genes important for T cell and mast cell development. The average expression of these 57 genes is 60, which we consider as the threshold for background. Therefore, genes whose expression is greater than 60 at at least one CT are included in the eigenvalue/pencil analysis and a total of 18,108 genes were analyzed in the end. For genes with multiple probes sets, only one probe was randomly selected and subject to the eigenvalue/pencil analysis, with exceptions for analysis described in Figure S2. The raw microarray data was normalized before the eigenvalue/pencil analysis by normalizing the probe intensity at every CT to the minimum probe value within the 48 time points so that the minimum gene expression value is always 1 for all genes. Oscillations with periods between 22∼26 hr, 10.5∼13.5 hr, 7∼9 hr, 3∼5 hr, 2∼2.5 hr are considered to be circadian, 12 hr, 8 hr, 4 hr and 2 hr genes.

The Eigenvalue/Pencil Approach

This approach was based upon the Loewner framework originally developed for linear systems with multiple inputs and outputs and later extended to linear parametric systems (Ionita and Antoulas, 2013, 2014). Mathematically, our method consists of the eigenvalue analysis of a pencil of matrices constructed from raw data. Specifically, the construction of a raw model of linear, time-invariant, discrete-time system driven by initial conditions is followed by dimension reduction using singular value decomposition (SVD) to identify the dominant oscillations.

First Step: We have a time series dataset expressed as $\mathbf{h} = [h(1), h(2) \cdots h(\mathrm{N})]$, and use it to construct a Hankel matrix as follows:

$$\mathbf{H}_{q,k,l} = \begin{bmatrix} h(q) & h(q+1) & \cdots & h(l) \\ h(q\ +\ 1) & h(q+2) & \cdots & h(l+1) \\ \vdots & \vdots & \ddots & \vdots \\ h(k-1) & h(k) & \cdots & h(k+l-q-1) \\ h(k) & h(k+1) & \cdots & h(k+l-q) \end{bmatrix} \tag{1}$$

Wherein $q \leq k$, $q \leq l$. In our case, the Hankel matrix can be represented as $\mathbf{H}_{1,R,R+1}$. Then we can define the quadruple $(\mathbf{E}_R, \mathbf{A}_R, \mathbf{B}_R, \mathbf{C}_R)$:

$$\mathbf{E}_R = \mathbf{H}_{1,R,R+1}(:, 1:R),\ \mathbf{A}_R = \mathbf{H}_{1,R,R+1}(:, 2:R+1),\ \mathbf{B}_R = \mathbf{H}_{1,R,R+1}(:, 1),\ \mathbf{C}_R = \mathbf{H}_{1,R,R+1}(1, 1:R) \tag{2}$$

This quadruple constitutes the raw model of the dataset **h**. This model is linear, time-invariant and discrete-time:

$$\mathbf{E}_R\mathbf{x}_R[n+1] = \mathbf{A}_R\mathbf{x}_R[n],\ \mathbf{y}_R[n] = \mathbf{C}_R\mathbf{x}_R[n],\ \mathbf{E}_R\mathbf{x}_R[0] = \mathbf{B}_R \tag{3}$$

wherein $n = 0, 1, 2\ldots$.

Second step: We use a model reduction approach to determine the dominant oscillations of the raw model. The raw model is reduced by using the SVD of $H_{1;R;R+1}$. We compute the following SVDs as follows:

$$[\mathbf{u}_1, \mathbf{s}_1, \mathbf{v}_1] = \mathrm{svd}\left(\begin{bmatrix} \mathbf{E}_R \\ \mathbf{A}_R \end{bmatrix}\right),\ [\mathbf{u}_2, \mathbf{s}_2, \mathbf{v}_2] = \mathrm{svd}([\mathbf{E}_R \quad \mathbf{A}_R]) \tag{4}$$

Then we choose the dimension r of the reduced system. Hence, we construct the projectors: $\mathbf{X} = \mathbf{u}_2(:, 1:r),\ \mathbf{Y} = \mathbf{v}_1(:, 1:r)$; and the reduced system matrices are:

$$\mathbf{E}_r = \mathbf{X}^T\mathbf{E}_R\mathbf{Y},\ \mathbf{A}_r = \mathbf{X}^T\mathbf{A}_R\mathbf{Y},\ \mathbf{C}_r = \mathbf{C}_R\mathbf{Y},\ \mathbf{B}_r = \mathbf{X}^T\mathbf{B}_R \tag{5}$$

The associated reduced model of dimension r is:

$$\mathbf{E}_r\mathbf{x}_r[n+1]=\mathbf{A}_r\mathbf{x}_r[n],$$

$$\mathbf{y}_r[n]=\mathbf{C}_r\mathbf{x}_r[n], \tag{6}$$

$$\mathbf{E}_r\mathbf{x}_r[0]=\mathbf{B}_r$$

Now, we have a reduced low-dimension system. We define $\mathbf{C}=\mathbf{C}_r$, $\mathbf{B}=[\mathbf{E}_r]^{-1}\mathbf{B}_r$, $\mathbf{A}=[\mathbf{E}_r]^{-1}\mathbf{A}_r$, then the approximation

$$\widehat{h}(n)=\mathbf{C}[\mathbf{A}]^{n-1}\mathbf{B} \tag{7}$$

To gather the information of oscillations, we perform eigenvalue decomposition (EVD) of the matrix pencil ($\mathbf{A}_r$ $\mathbf{E}_r$), the same way as we perform EVD of $\mathbf{A}$, then we have

$$[\mathbf{E}_r]^{-1}\mathbf{A}_r=\mathbf{V}_r\Lambda_r[\mathbf{V}_r]^{-1} \tag{8}$$

Wherein $\mathbf{V}_r=[\boldsymbol{v}_1,\ldots,\boldsymbol{v}_r]$, $\Lambda_r=\mathrm{diag}[\lambda_1,\ldots,\lambda_r]$. Then the approximation can be decomposed as

$$\widehat{h}(n)=\sum\nolimits_{i=1}^{r}\mathbf{C}\boldsymbol{v}_i[\lambda_i]^{n-1}\boldsymbol{v}_i^H\mathbf{B}=\sum\nolimits_{i=1}^{r}P_i*[\lambda_i]^{n-1} \tag{9}$$

wherein P_i is complex amplitude of the i^{th} oscillation. Because P_i and λ_i are all complex number that it can be represent as

$$P_i*[\lambda_i]^n=\alpha_i*e^{\sigma_i n}*e^{j(\omega_i n+\theta_i)} \tag{10}$$

wherein α_i is the amplitude, σ_i is the decay (grow) rate, ω_i is the frequency and θ_i is the phase of the i^{th} oscillation.

Identifying Dominant Biological Oscillations

Next, we used *Bmal1* time-series microarray data (Hughes et al., 2009) as an example to demonstrate the application of eigenvalue/pencil to identify dominant superimposed oscillations. We calculated the oscillations of the reduced model with r = [3, 5, 7, 9], in addition to the raw model without dimension reduction. The values of pole λ_i under different dimension reduction (and raw model) are shown in the following table for the *Bmal1* gene.

r = 3	r = 5	r = 7	r = 9	Raw model
1.0012	1.0011	1.0011	1.0011	1.0053
0.9672 + 0.2522i	0.9673 + 0.2520i	0.9674 + 0.2519i	0.9674 + 0.2521i	0.9684 + 0.2599i
0.9672 – 0.2522i	0.9673 – 0.2520i	0.9674 – 0.2519i	0.9674 – 0.2521i	0.9684 – 0.2599i
	0.8720 + 0.5137i	0.8761 + 0.5151i	0.8805 + 0.5150i	0.8473 + 0.4592i
	0.8720 – 0.5137i	0.8761 – 0.5151i	0.8805 – 0.5150i	0.8473 – 0.4592i
		0.6218 + 0.7802i	0.6357 + 0.7685i	0.7932 + 0.7400i
		0.6218 – 0.7802i	0.6357 – 0.7685i	0.7932 – 0.7400i
			–0.3691 + 0.8542i	–0.3526 + 1.1144i
			–0.3691 – 0.8542i	–0.3526 – 1.1144i

The striking feature of this analysis is that the pole values of oscillations of large periods remain mostly unchanged as more oscillations are added by using higher reduced models (the top four oscillations revealed by 9th reduced model corresponds to T = 24.65, 11.86, 7.14 and 3.17 hr as shown in Figure S1F). These data suggest that 9th order model is a good trade-off between the fitness of the model to the raw data and the likelihood that the oscillations of newly added smaller periods are noise rather than real biological oscillations. This assertion is further supported by the examination of superimposed oscillations from different probe sets against the same gene (Figures S2A–S2C). Therefore, we believe the 9th reduced model, which can identify up to four different oscillations, is the optimal model to reveal robust novel oscillations.

siRNA Transient Transfections

MEFs were transfected with 10μM of different siRNAs for 24∼48 hr with Lipofectamine RNAiMAX reagents (Life technologies) per the manufacturer's instructions. Source of siRNA are as follows: siGENOME Non-Targeting siRNA pool (Dharmacon, D-001206-13-05), siGENOME SMARTpool ARNTL (Dharmacon, L-040483-01-0005), siGENOME SMARTpool XBP1 (Dharmacon, L-040825-00-0005).

Immunoblot

Immunoblot analyses were performed as described previously (Zhu et al., 2015). Briefly, proteins separated by 4∼20% gradient SDS-PAGE gels (Biorad) were transferred to nitrocellulose membranes, blocked in TBST buffer supplemented with 5% bovine serum

albumin (BSA) and incubated overnight with primary antibody at 4°C. Blots were incubated with an appropriate secondary antibody coupled to horseradish peroxidase at room temperature for 1 hr, and reacted with ECL reagents per the manufacturer's (Thermo) suggestion and detected on X-ray film by autoradiography. The antibodies used in immunoblot are provided in Key Resources Table.

qRT-PCR

Total mRNA was isolated from murine embryonic fibroblasts (MEFs) or liver with PureLink RNA mini kit (Life Technologies) per the manufacturer's instructions. Reverse transcription was carried out using 5μg of RNA using Superscript III (Life Technologies) per the manufacturer's instructions. For gene expression analyses, cDNA samples were diluted 1/30-fold (for all other genes except for 18sRNA) and 1/900-fold (for 18sRNA). qPCR was performed using the Taqman or SYBR green system with sequence-specific primers and/or the Universal Probe Library (Roche). All data were analyzed with 18S or β-Actin as the endogenous control. All qPCR primer sequences are shown in Table S6.

ChIP-qPCR

Liver tissue was isolated and flash frozen at designated CTs. Chromatin was isolated using the SimpleChIP Enzymatic Chromatin IP Kit (Cell Signaling) and performed per the manufacturer's suggestion. Briefly, mouse liver samples were submerged in PBS + 1% formaldehyde, cut into small (~1 mm^3) pieces with a razor blade and incubated at room temperature for 20 min. Fixation was stopped by the addition of 0.125 M glycine (final concentration). The tissue pieces were then treated with a TissueTearer and finally spun down and washed twice in PBS. Chromatin was isolated by the addition of lysis buffer, followed by disruption with a Dounce homogenizer. Lysates were enzymatically digested with *MNase* and the DNA was digested to an average length of 145 bp. Genomic DNA (Input) was prepared by treating aliquots of chromatin with RNase, Proteinase K and heated for reverse-crosslinking, followed by ethanol precipitation. Pellets were resuspended and the resulting DNA was quantified on a NanoDrop spectrophotometer. An aliquot of chromatin (5 μg) was precleared with protein A agarose beads (Invitrogen). Genomic DNA regions of interest were isolated using 2 μg of antibody. Complexes were washed, eluted from the beads with SDS buffer, and subjected to RNase and proteinase K treatment. Crosslinking were reversed by incubation overnight at 65°C, and ChIP DNA was purified by phenol-chloroform extraction and ethanol precipitation. For ChIP-qPCR on MEFs, cells were fixed with 1% formaldehyde for 20mins and ChIP was performed essentially the same way. XBP1 (M186) (Santa Cruz) and (poly6195) (Biolegend) antibodies were used for XBP1 ChIP-qPCR. All ChIP-qPCR primer sequences are shown in Table S6.

Cloning

XBP1s-pHAGE

The XBP1s overexpression plasmid is a generous gift from Dr. Xi Chen at Baylor College of Medicine and made in-house in Dr. Xi Chen's lab.

Eif2ak3-dluc

An 1026bp long mouse *Eif2ak3* promoter (−754bp to +272bp) was PCR amplified from NIH 3T3 cells genomic DNA using the following primers: forward primer: ATAGAGCTCAAACCAACCGGGAGACTTAAT; reverse primer: ATACTCGAGCCAGCAGCAGG AACAGAA and subcloned into pGL4.16[luc2CP/Hygro] vector (E6711, Promega), which encodes for a destabilized luciferase gene. All sequences were confirmed by sequencing.

Eif2ak3-dluc with Mutated XBP1s Binding Site

To mutate CCACGTC to CCAAAAA, site-directed mutagenesis was performed using the Q5 Site-Directed Mutagenesis Kit (E0554S) (NEB) with the following primers: forward primer: CAGTGGCTGAtttttGGCCGGGCAGCTC; reverse primer: CCACCTGAGTGA CAGCCT per the manufacturer's suggestion. All sequences were confirmed by sequencing.

Eif2ak3-dGFP

An 1026bp mouse *Eif2ak3* promoter (−754bp to +272bp) was PCR amplified from NIH 3T3 cells genomic DNA using the following primers: forward primer: ATAATCGATAAACCAACCGGGAGACTTAAT; reverse primer: ATAACTAGTCCAGCAGCAGGAACAGAA and subcloned into pGreenfire-mCMV-dscGFP-EF1-Puro lentiviral vector (TR010PA-P, System Biosciences), which encodes for a destabilized GFP gene. All sequences were confirmed by sequencing.

Sec23b-dluc

An 654bp long mouse *Sec23b* promoter (−513bp to +141bp) was PCR amplified from NIH 3T3 cells genomic DNA using the following primers: forward primer: ATAATCGATAGCACAGAAACCACAGCA; reverse primer: ATAACTAGTTTCACCATTGCAGAGCCA and subcloned into pGL4.16[luc2CP/Hygro] vector (E6711, Promega), which encodes for a destabilized luciferase gene. All sequences were confirmed by sequencing.

Sec23b-dluc with Mutated XBP1s Binding Site

To mutate CCACCTC to CCAAAAA, site-directed mutagenesis was performed using the Q5 Site-Directed Mutagenesis Kit (E0554S) (NEB) with the following primers: forward primer: ACTGTGAGCTttttTGGACTTGGCGGTGG; reverse primer: CGATTGGTCA CCGCTCCG per the manufacturer's suggestion. All sequences were confirmed by sequencing.

Transient Luciferase Assay

MEFs were co-transfected with internal control vector pRL-TK and *Eif2ak3*-dluc, *Eif2ak3*-dluc with mutated XBP1s binding site, *Sec23b*-dluc or *Sec23b*-dluc with mutated XBP1s binding site using Lipofetamine 2000 for 24 hr before transfected with increasing

amount of XBP1s overexpression vector using Lipofetamine 2000 for another 24 hr. After that, the cells were lysed with 50μl of 1x passive lysis buffer and subject to dual-reporter luciferase assay per the manufacturer's suggestion. The Firefly luciferase signal was normalized to that of Renilla luciferase signal.

Generation of Stable MEFs Lines

To generate *Eif2ak3*-dluc or *Eif2ak3*-dluc with mutated XBP1s binding site stably expressing MEFs, MEFs cultured in 15cm dish were transiently transfected with *Eif2ak3*-dluc or *Eif2ak3*-dluc with mutated XBP1s binding site plasmids for 48 hr. After that, cells were cultured in the presence of 200μg/ml hygromycin to select for resistant cells. To generate stable *Eif2ak3*-dGFP cells, *Eif2ak3*-dGFP lentivirus were first generated by co-transfecting 293TN producer cells with *Eif2ak3*-dGFP, pMD2G and psPAX2 plasmids with the ratio of 3:2:1 for 48 hr and collecting supernatant. Virus were filtered with a 0.45μM syringe filter. MEFs were subsequently infected with *Eif2ak3*-dGFP encoding lentivirus in the presence of 4 μg/ml polybrene for 48 hr and cultured in the presence of 4 μg/ml puromycin to select for stable cells. Cells were subject to multiple rounds of virus infections to increase the percentage of GFP positive cells.

Real-Time Luminescence Assay

Stable *Eif2ak3*-dluc or *Eif2ak3*-dluc with mutated XBP1s binding site MEFs were cultured in DMEM (4.5g/L glucose) supplemented with 10% FBS and treated with 25ng/ml of Tu (high glucose DMEM with 10% FBS) or glucose depletion (high glucose DMEM with 10% dialyzed FBS) for 2 hr before subjected to real-time luminescence assay using a Lumicycle (Actimetrics) as previously described (Zhu et al., 2015). Briefly, after Tu or GD treatment, MEFs were washed with 1x PBS and cultured with DMEM (4.5g/L glucose) supplemented with 0.1 mM Luciferin and 10mM HEPES buffer in 35 mm tissue culture dishes in the absence of serum and transferred immediately to Lumicycle for real-time luminescence analysis. Periods of oscillation were identified by embedded Periodogram function. For siRNA treated MEFs, MEFs were transfected with non-targeting or *Xbp1* siRNA for 48 hr before subject to Tu or GD shock and real-time luminescence assay as described above.

Time-Lapse Microscopy

Time-lapse microscopy was performed on *Eif2ak3*-dGFP cells using IncuCyte Live Cell Analysis System (Essen Bioscience). *Eif2ak3*-dGFP was subject to imaging using 300ms integration time at 30min interval. During the imaging, the cells were cultured in serum free medium. GFP intensity for single cells (cell lineages) was subsequently quantified automatically by automated image processing software CellProfiler (version 2.2.0) (Carpenter et al., 2006). We quantified a total of 89 single cell/cell lineages, collected from 12 different fields of views from 6 different wells from three independent imaging experiments and dominant and superimposed oscillations were subsequently identified by the eigenvalue/pencil approach. The CellProfiler pipeline used for identification, quantification and tracking of single cells as well as raw images are available upon request. The videos were generated using VirtualDubMod 1.5.10 (https://sourceforge.net/projects/virtualdubmod/files/) using indicated frame per second (fps). The raw data were subject to polynomial detrend (n = 4∼7) and eigenvalue/pencil method were applied to uncover top superimposed oscillations from mathematically detrended data.

Measurement of Plasma Glucose and Insulin

Plasma glucose level was measured by a glucometer and plasma insulin level was measured by a commercial insulin ELISA kit (EZRMI-13K, Millipore) per the manufacturer's instructions.

Metabolic Profiling Using CLAMS

Calorimetry (Columbus Instruments) was used for real time measuring of Respiratory Exchange Ratio (RER). Mice fed ad libitum (n = 7 biological replicates) or restricted fed during the day (ZT3 to ZT11) (n = 8 biological replicates) were acclimated to the chambers for at least one week and food intake was monitored for 5 days under a 12 hr light/dark cycle. Data were collected for VO2 consumed and VCO2 released and RER was calculated as VCO2/VO2.

QUANTIFICATION AND STATISTICAL ANALYSIS

Data Analysis by ARSER, RAIN and JTK_CYCLE

To compare our eigenvalue/pencil method with other methods commonly used to identify cycling transcripts in the circadian field, we analyzed the same 18,108 hepatic genes to uncover 12 hr cycling genes using three separate methods: ARSER (Yang and Su, 2010), RAIN (Thaben and Westermark, 2014) and JTK_CYCLE (Hughes et al., 2010) with respective algorithms described in their publications. However, unlike our eigenvalue/pencil method, which does not require a pre-assignment of periods range, all three methods need the user to assign a period range. For identifying novel ∼12 hr cycling genes, we used a loose criteria of period range from 10 to 14 hr. We additionally used two different p value cut-offs ($p < 0.01$ and $p < 0.05$) for selecting high confidence ∼12 hr cycling genes. The detailed results are provided in Table S3. The data analysis was performed in Bioconductor (3.4) for RAIN (http://www.bioconductor.org/packages/release/bioc/html/rain.html) and in MetaCycle for both JTK_CYCLE and ARSER (https://github.com/gangwug/MetaCycle).

Gene Ontology Analysis

DAVID (Huang et al., 2009) (https://david.ncifcrf.gov) was used to perform Gene Ontology analysis. Briefly, gene names were first converted to DAVID-recognizable IDs using Gene Accession Conversion Tool. The updated gene list was then subject to GO analysis using *Mus musculus* as background and with Functional Annotation Chart function. KEGG_PATHWAY, SP_PIR_KEYWORDS, GOTERM_BP_FAT and GOTERM_CC_FAT were used as GO categories for all GO analysis. Only GO terms with p value smaller than 0.05 were included for further analysis.

Post Hoc Analysis of Hepatic SILAC Data

The time series hepatic mass spectrometry-based proteomics data from mice kept under constant darkness for 45 hr was previously published (n = 3 triplicates at each CT) (Robles et al., 2014). We first normalized the raw data by calculating the $\log_2$ (fold change over mean) at each CT for each sample and then averaged the normalized values of the three replicates at each CT. Upon examining the normalized data, we observed noticeable baseline changes in most reported protein oscillations. Therefore, we then subjected the normalized data to polynomial detrend (n = 3). Due to the relatively poor resolution of the dataset (at 3 hr interval), we decided against the use of our eigenvalue/pencil approach but rather employed a more simplified but well-established CircWave software to only characterize proteins cycling with a dominant 12 hr period (Keller et al., 2009). The normalized and detrended dataset was subject to CircaWave analysis (CircWave batch 3.3). A less stringent cutoff of p value = 0.1 was used because we reason since most 12 hr rhythms of gene expression are superimposed by other oscillations; a less stringent criterion will be more likely to identify 12 hr cycling proteins with asymmetrical 12 hr peaks caused by the superimposition. The $\log_2$ normalized and detrended data for proteins with 12 hr oscillations are provided in Table S5. For simplicity, only the mean values at each CT are provided. Heatmaps were generated by Gene Cluster 3.0 and TreeView 3.0 alpha 3.0 on polynomial detrended data.

Post Hoc Analysis of Hepatic Metabolomic Data

The time series hepatic metabolomics data from mice entrained under 12 hr light/12 dark schedule for 24 hr was previously published (n = 5 biological replicates at each CT) (Eckel-Mahan et al., 2013). Only the mean value of each metabolite was reported in the original study. Like the SILAC dataset, due to the poor resolution and short duration of the dataset (at 4 hr interval for a total of only 24 hr), we again employed CircWave method to only characterize metabolites cycling with a dominant 12 hr period. For this analysis, a cutoff of p value = 0.1 was also used. Heatmaps were generated by Gene Cluster 3.0 and TreeView 3.0 alpha 3.0.

Post Hoc Analysis of C. elegans Microarray

In this study (van der Linden et al., 2010), *C. elegans* were entrained by either 12 hr light/12 dark or 12 hr warm temperature (25°C)/12 hr cold temperature (15°C) conditions. We specifically analyzed the microarray data under 25°C/15°C entrained as well as 15°C free-run conditions. The raw microarray data reported in experiment 3 was polynomial detrended (n = 2) before subject to CircWave analysis to identify dominant 12 hr cycling genes ($p \leq 0.1$). The *C. elegans* ortholog of mammalian genes were identified using NCBI AceView tool (https://www.ncbi.nlm.nih.gov/IEB/Research/Acembly/index.html). Heatmaps were generated by Gene Cluster 3.0 and TreeView 3.0 alpha 3.0 on polynomial detrended data.

Gene Set Enrichment Analysis

Gene Set Enrichment Analysis (GSEA) was performed using GSEA 2.0. Gene sets of top ~12 hr and ~24 hr cycling genes (at both mRNA and protein level) were provided in Table S5. Human NASH and hepatic steatosis microarray data were obtained from published database (Ahrens et al., 2013). 1000 permutations were performed using phenotype permutation option. Weighted and signal2noise were selected for Enrichment Statistic and Metric for ranking genes, respectively. Normalized Enrichment Score (NES) and FWER p value were provided for each analysis.

Statistical Analysis

Statistical analysis was conducted using GraphPad Prism 7 software. All data were tested for normal distribution of variables. All normally distributed data were displayed as means ± standard error of the mean (SEM) unless otherwise noted. Measurements between two groups were performed with an unpaired Student's t test.

DATA AND SOFTWARE AVAILABILITY

Raw and Cell Profiler-processed images for single cell Eif2ak3-dGFP recordings were deposited into Mendeley Data with URL: http://dx.doi.org/10.17632/wk8sfwbfw4.1.

Cell Metabolism, Volume *25*

Supplemental Information

A Cell-Autonomous Mammalian 12 hr Clock Coordinates Metabolic and Stress Rhythms

Bokai Zhu, Qiang Zhang, Yinghong Pan, Emily M. Mace, Brian York, Athanasios C. Antoulas, Clifford C. Dacso, and Bert W. O'Malley

Figure S1. Zhu et al.

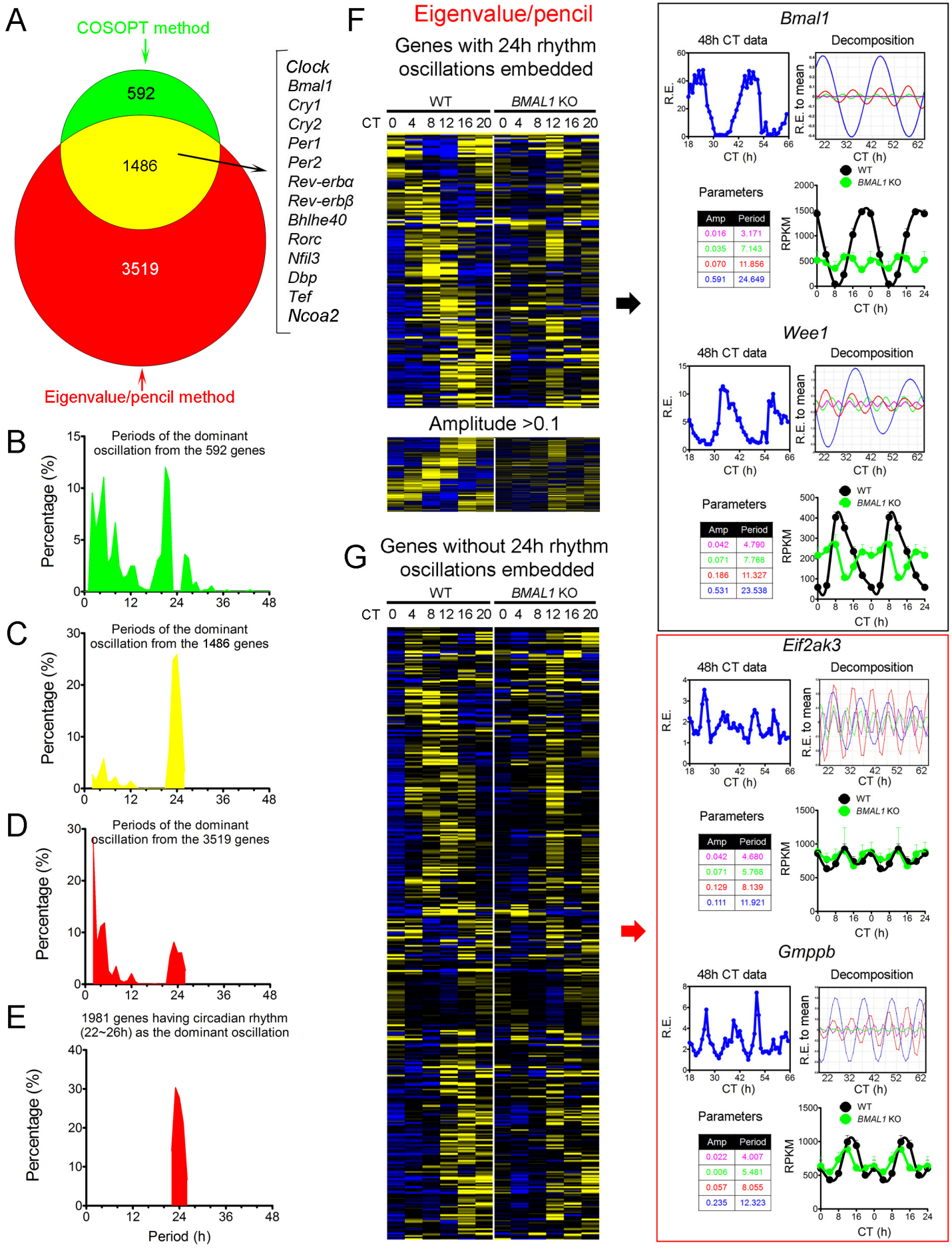

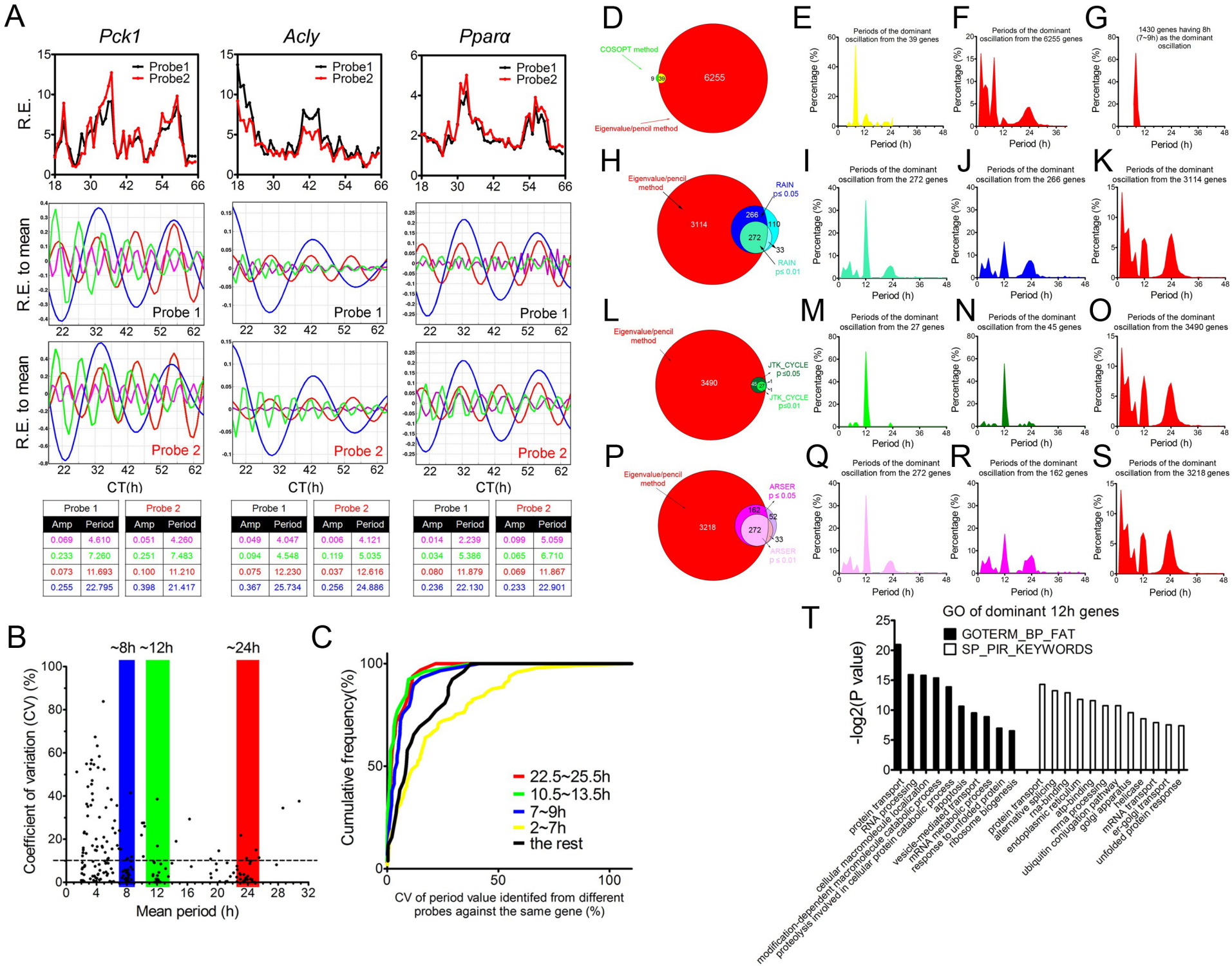

Probe 1		Probe 2	
Amp	Period	Amp	Period
0.069	4.610	0.051	4.260
0.233	7.260	0.251	7.483
0.073	11.693	0.100	11.210
0.255	22.795	0.398	21.417

Probe 1		Probe 2	
Amp	Period	Amp	Period
0.049	4.047	0.006	4.121
0.094	4.548	0.119	5.035
0.075	12.230	0.037	12.616
0.367	25.734	0.256	24.886

Probe 1		Probe 2	
Amp	Period	Amp	Period
0.014	2.239	0.099	5.059
0.034	5.386	0.065	6.710
0.080	11.879	0.069	11.867
0.236	22.130	0.233	22.901

Figure S2.Zhu et al.

Figure S3. Zhu et al.

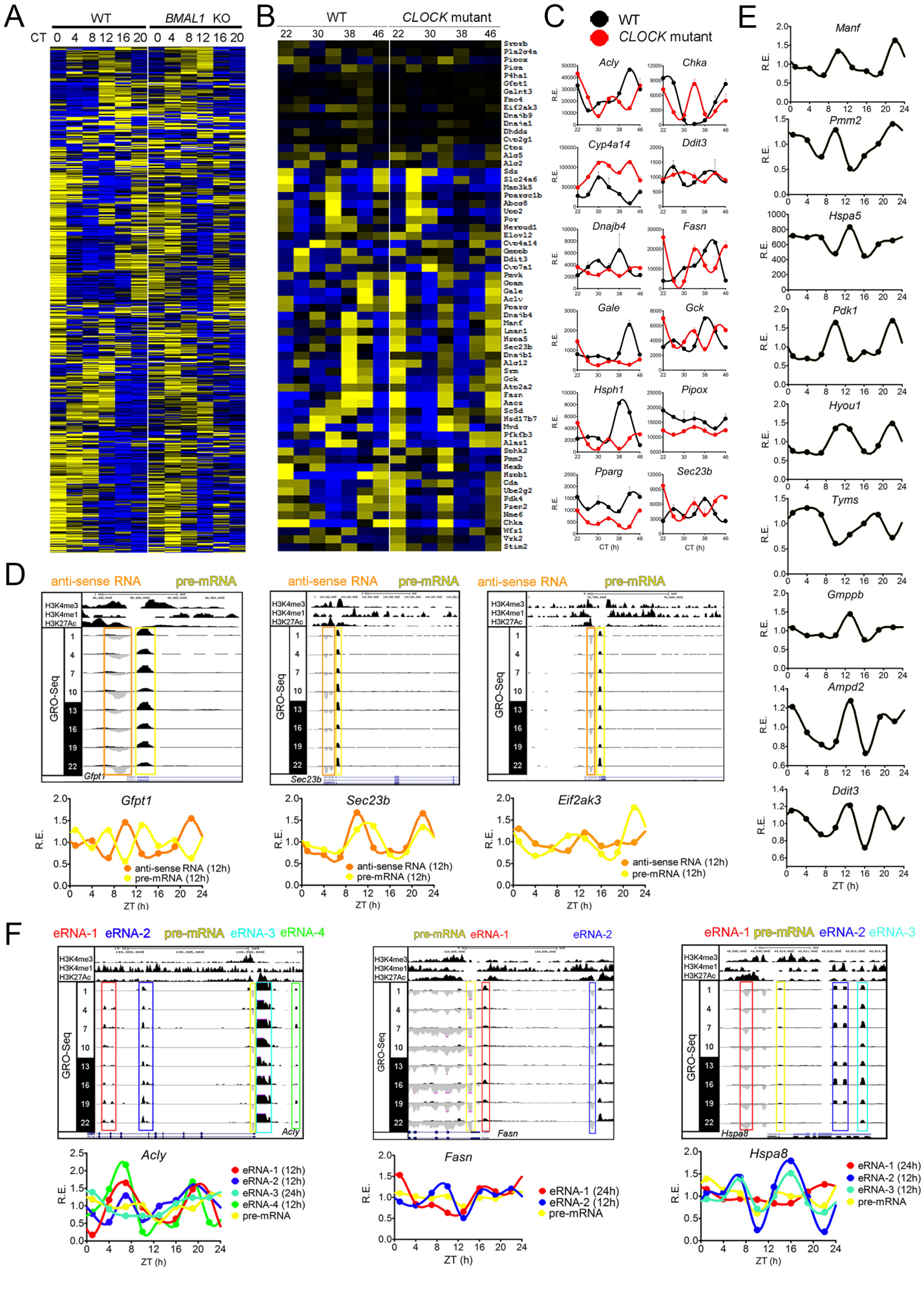

Figure S4. Zhu et al.

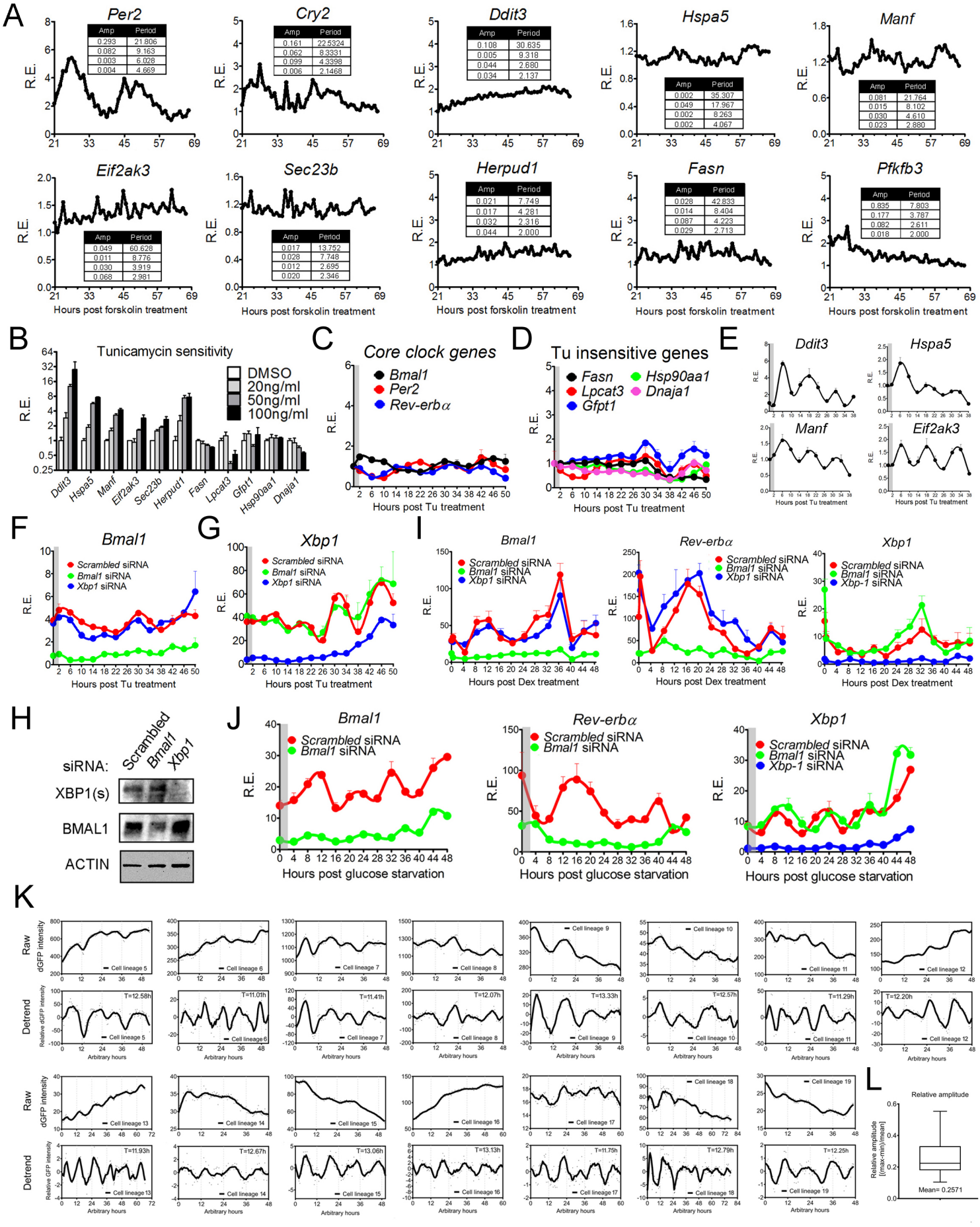

Figure S5. Zhu et al.

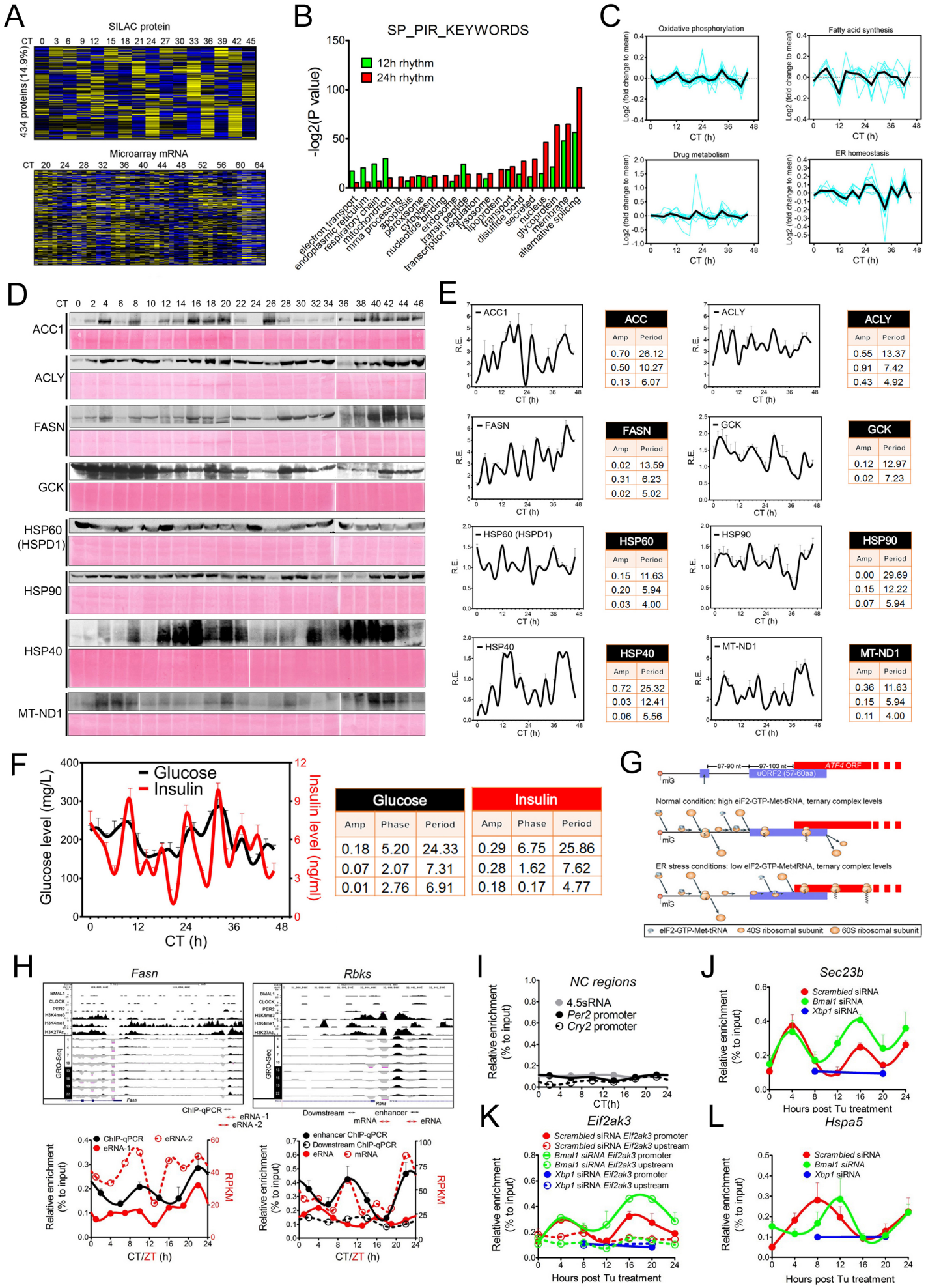

Figure S6. Zhu et al.

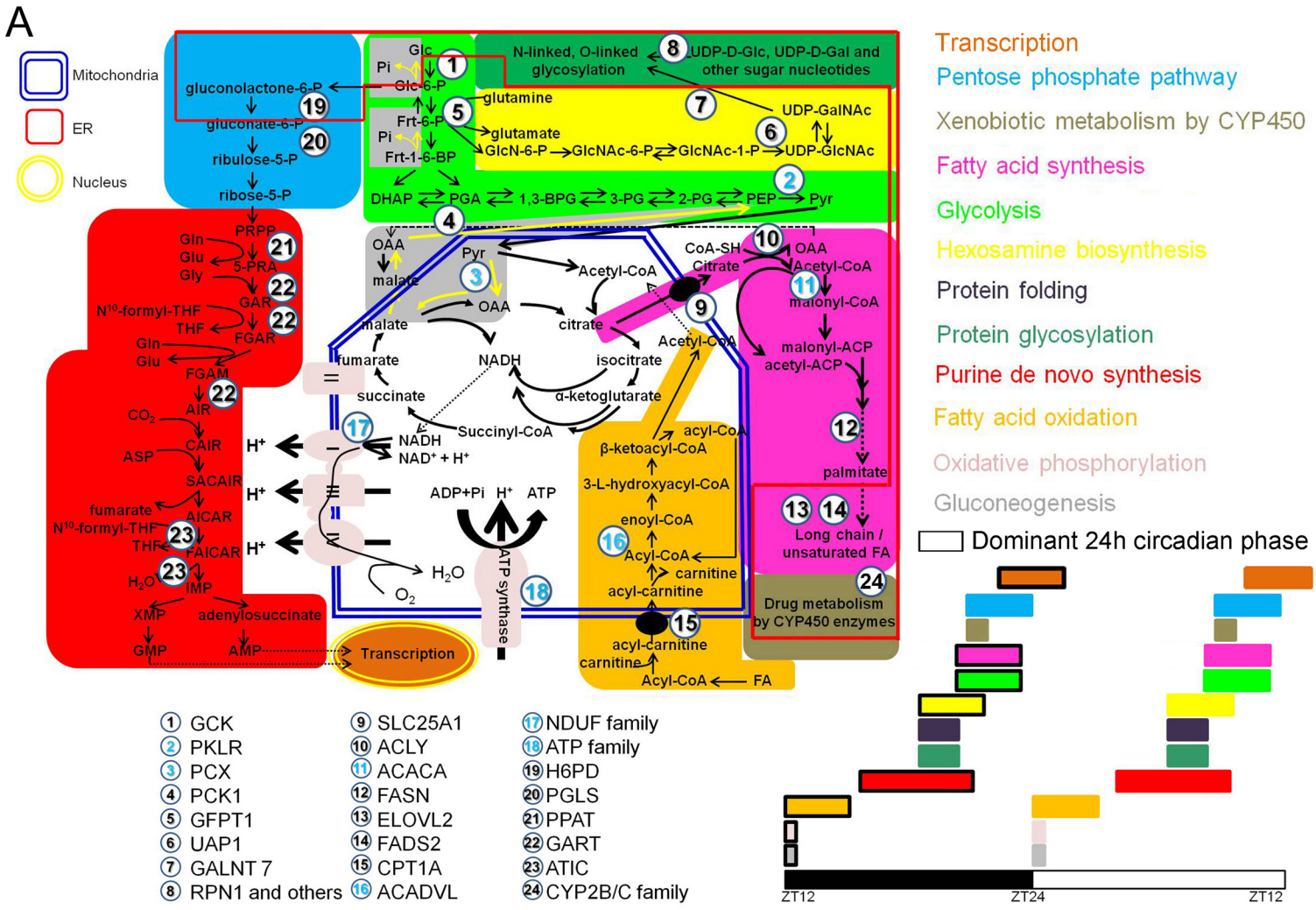

B

RBKS

ATP + D-ribose ↔ ADP + D-ribose 5-phosphate

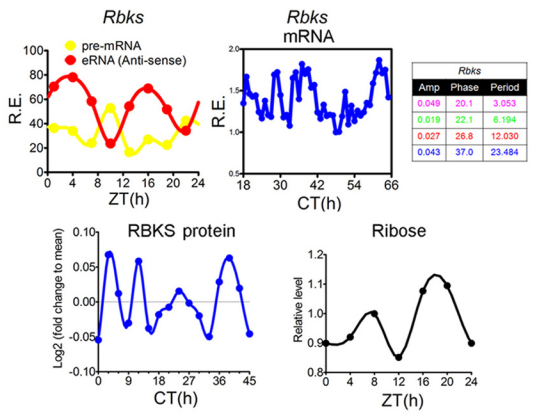

Rbks		
Amp	Phase	Period
0.049	20.1	3.053
0.019	22.1	6.194
0.027	26.8	12.030
0.043	37.0	23.484

C

SUCLA2

Succinyl CoA + Pi + NDP ↔ Succinate + CoA + NTP

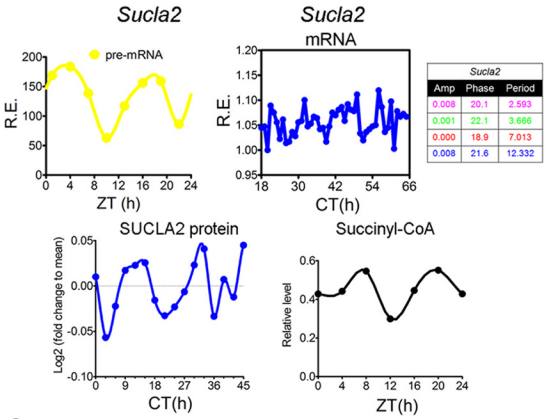

Sucla2		
Amp	Phase	Period
0.008	20.1	2.593
0.001	22.1	3.666
0.000	18.9	7.013
0.008	21.6	12.332

D

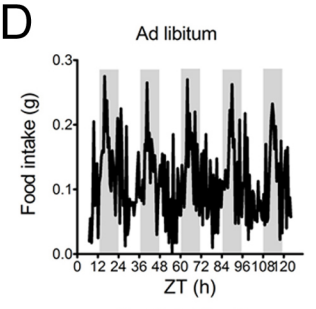

E

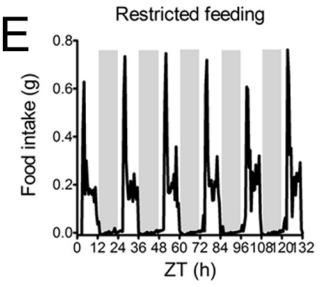

F

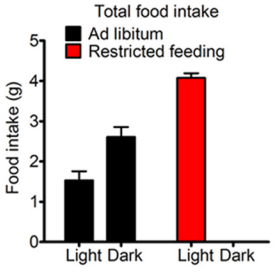

G

Mouse #1	
Amp	Period
0.0012	1.852
0.0196	11.803
0.0228	25.276
0.8295	mean

Mouse #2	
Amp	Period
0.0178	1.442
0.0004	2.250
0.0062	12.412
0.0193	24.196
0.8622	mean

Mouse #3	
Amp	Period
0.0060	2.303
0.0095	2.873
0.0190	11.815
0.0248	24.744
0.8495	mean

Mouse #4	
Amp	Period
0.0030	2.171
0.0002	6.568
0.0045	10.599
0.0424	23.761
0.8625	mean

Mouse #5	
Amp	Period
0.0004	1.405
0.0065	1.831
0.0065	12.142
0.0310	24.128
0.0033	58.888
0.8677	mean

Mouse #6	
Amp	Period
0.0027	3.613
0.0012	7.850
0.0064	11.720
0.0238	23.914
0.8931	mean

Mouse #7	
Amp	Period
0.0020	5.009
0.0120	8.409
0.0085	12.481
0.0238	24.696
0.9080	mean

H

Mouse #1	
Amp	Period
0.0037	4.828
0.0116	7.424
0.0256	7.996
0.0010	20.277
0.0817	23.926
0.8843	mean

Mouse #2	
Amp	Period
0.0112	4.795
0.0078	6.020
0.0196	7.990
0.0072	12.380
0.0866	23.840
0.8913	mean

Mouse #3	
Amp	Period
0.0090	3.453
0.0093	4.792
0.0081	6.096
0.0170	7.973
0.0722	23.830
0.8941	mean

Mouse #4	
Amp	Period
0.0076	3.438
0.0131	5.998
0.0151	7.942
0.0185	12.204
0.0904	23.770
0.9236	mean

Mouse #5	
Amp	Period
0.0083	4.821
0.0102	5.999
0.0220	7.962
0.0841	23.857
0.0080	55.522
0.8897	mean

Mouse #6	
Amp	Period
0.0085	3.427
0.0099	5.983
0.0149	7.954
0.0283	12.435
0.0891	23.819
0.9412	mean

Mouse #7	
Amp	Period
0.0080	3.440
0.0038	4.053
0.0089	5.991
0.0190	8.018
0.0899	24.061
0.9412	mean

Mouse #8	
Amp	Period
0.0057	4.792
0.0067	6.003
0.0206	8.031
0.0094	12.034
0.0866	24.030
0.8936	mean

Figure S7. Zhu et al

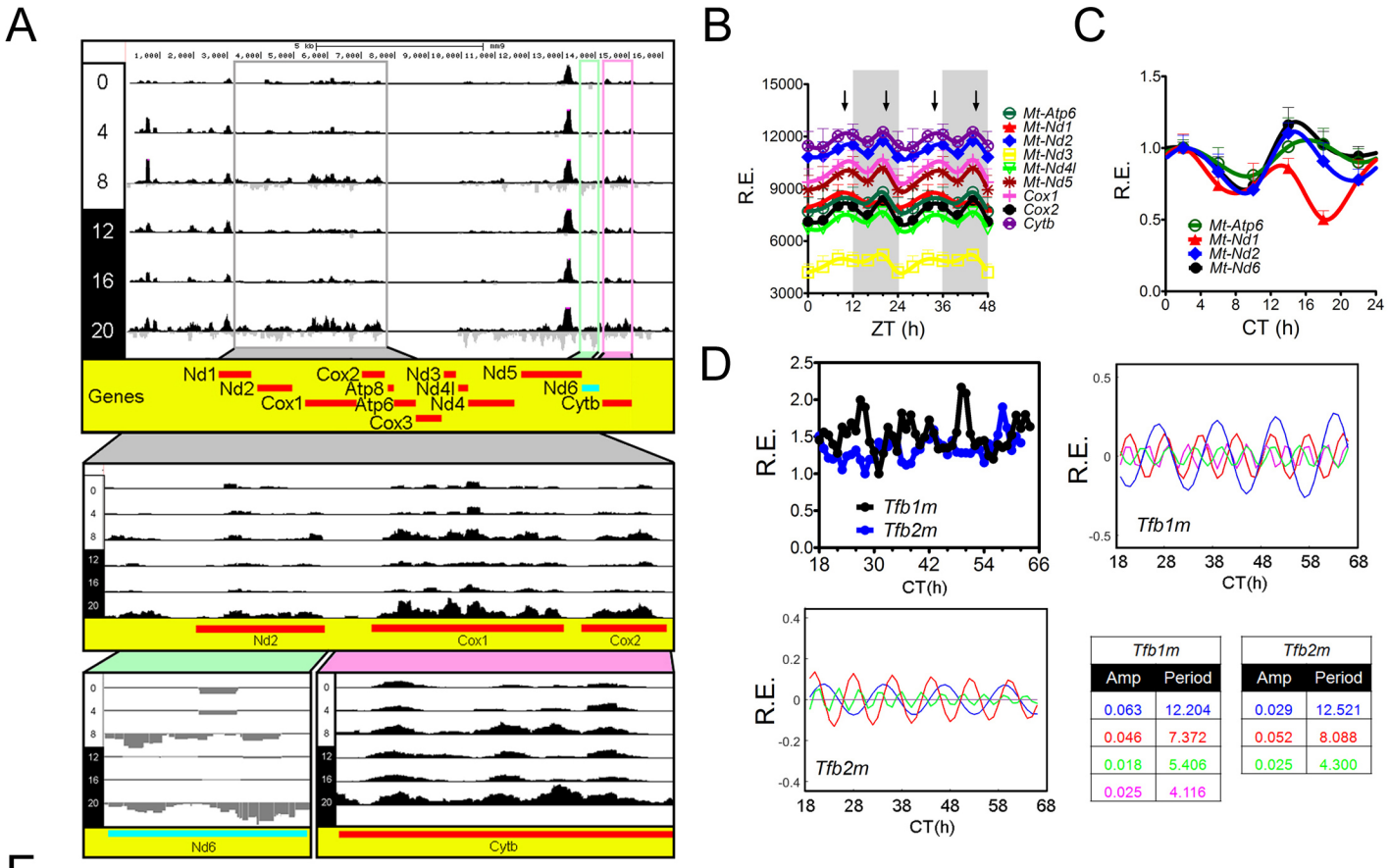

Tfb1m	
Amp	Period
0.063	12.204
0.046	7.372
0.018	5.406
0.025	4.116

Tfb2m	
Amp	Period
0.029	12.521
0.052	8.088
0.025	4.300

E

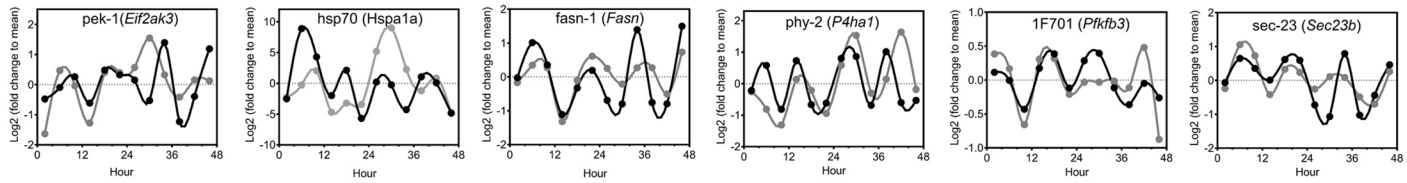

F

Top ~12h cycling gene identified in mouse liver

Gene names in mouse	Period	Relative amplitude	Ortholog gene in C. elegans	Having ~12h rhythmicity in C. elegans?
Rgs16	10.680	1.085	rgs-7	Yes
Nipal1	11.758	0.790	nipa-1	Yes
Hspa1b	11.823	0.785	hsp-70	Yes
Bag3	11.594	0.667	wwp-1	Yes
Nr1d1	11.532	0.653	nhr-85	No
Mfsd2a	11.267	0.604	XF291	No
Tsku	11.340	0.584	tol-1	Yes
Cwf19l2	11.197	0.569	B0361.2	Yes
Dbp	11.647	0.520	ces-2	No
Fasn	12.711	0.518	fasn-1	Yes
Usp2	11.271	0.484	4H525	Yes

G

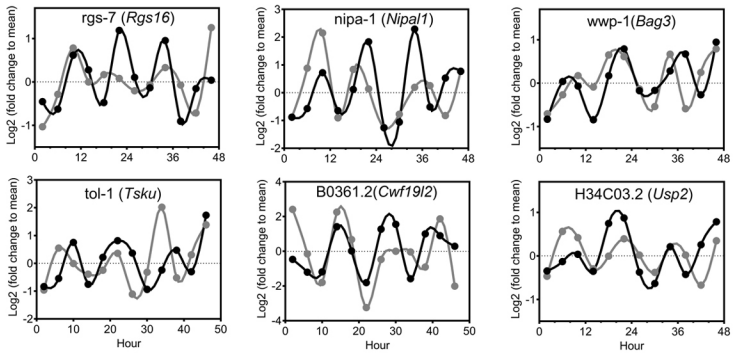

H

Top circadian gene identified in mouse liver

Gene names in mouse	Period	Relative amplitude	Ortholog gene in C. elegans	Having circadian rhythmicity in C. elegans?
Mfsd2a	22.615	1.448	XF291	No
Usp2	23.260	1.159	4H525	No
Lrp1	24.142	1.155	lrp-2	No
Ccrn4l	23.031	1.084	ccr-4	No
Dbp	23.396	1.081	ces-2	Yes for one rep
Nr1d1	23.283	0.993	nhr-85	No
AW107722	22.799	0.984	not found	N/A
Lpin1	23.235	0.975	lpin-1	No
Gm129	23.321	0.950	not found	N/A
E030016H06Rik	24.856	0.877	not found	N/A

I

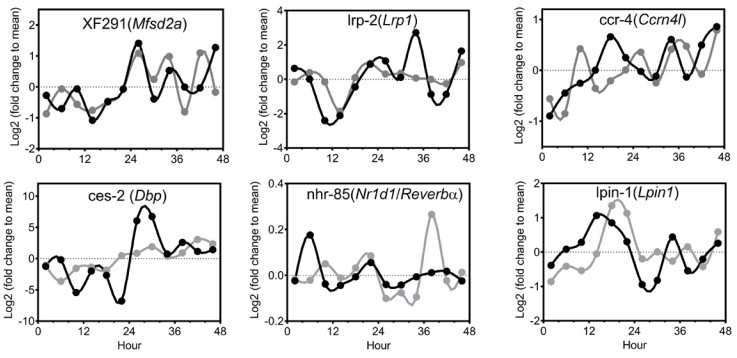

SUPPLEMENTAL FIGURES:

Figure S1. The eigenvalue/pencil method can robustly identify circadian genes, related to Figure 1.

(A) Venn diagram comparison of the number of circadian genes identified via the eigenvalue/pencil or the COSOPT method described in (Hughes et al., 2009). Core clock genes were identified by both methods. **(B-E)** The distributions of the periods of the dominant oscillations from the 592 circadian genes only identified by the COSOPT method **(B)**, the 1,486 commonly found circadian genes **(C),** the 3,519 circadian genes only identified by the eigenvalue approach **(D)** or the dominant 1,981 circadian genes identified by the eigenvalue approach (**E**). **(F,G)** All 18,108 genes analyzed by the eigenvalue/pencil method are divided in two groups based upon the presence **(F)** or absence **(G)** of superimposed ~24h oscillations. For mRNA with embedded ~24h oscillations, those with the relative amplitude of 24h oscillation larger than 0.1 are further selected. Heatmaps of mRNA expression in wild-type (WT) or *BMAL1*$^{-/-}$ (*BMAL1* KO) mice from a published RNA-Seq database at different CTs (Yang et al., 2016) are shown. Further, raw microarray data used for deconvolution, deconvoluted plots, identified parameters for different oscillations and mRNA expression of representative genes (*Bmal1* and *Wee1* represent genes with 24h oscillation and *Eif2ak3* and *Gmppb* represent genes without 24h oscillation in WT mice) in wild-type (WT) or *BMAL1* knock-out (*KO*) mice are shown on the right (n=4). The RNA-Seq data are double plotted for better visualization.

Figure S2. Eigenvalue/pencil approach identifies wide prevalence of 8h and 12h hepatic genes, which are robust oscillations, related to Figure 1.

(A-C) To tested the robustness of the identified oscillations, we compared the oscillations derived from different microarray probes against the same gene. A 60-gene cassette containing multiple microarray probes per gene (Hughes et al., 2009) was randomly selected and subjected to mathematical decomposition. We reasoned that if oscillations from a given gene were robust, then the identified period lengths should be similar, that is with smaller coefficient of variation (CV), among different probe datasets. Likewise,

identified oscillations of largely disparate periods (larger CV value) from different probes are likely to stem from technical noise and are less likely to represent real biological oscillations. Using this rationale, we found that 8h, 12h and 24h are the most robust oscillations as approximately 90% of these oscillations have CV values less than 0.1 **(A-C).** In contrast, oscillations with periods in between (60% with CV <0.1) and with shorter periods (<7h) (only 45% with CV<0.1) were found to be less robust **(A-C)**. Combined with the observation that oscillations of larger periods (8~24h) remain mostly unchanged as more oscillations are added by using higher reduced models (See Supplemental Experimental Procedures), we showed that in addition to the well-characterized circadian rhythm, oscillations with periods of 12h and 8h are robust rhythms with potential biological significance. Detailed figure legends: **(A)** Representative deconvolution of metabolism (*Pck1*, *Acly*, *Pparα*) genes mRNA expression by the eigenvalue/pencil method. For every gene, mRNA expressions detected by two different probe sets are analyzed by the eigenvalue/pencil method. Top row represents raw microarray data (Hughes et al., 2009); second and third rows plot revealed superimposed oscillations for different probe sets; and the fourth row illustrates the amplitudes and periods of different oscillations for different probe sets with the color matching the different oscillations depicted in the second and third row. **(B)** Coefficient of variation (CV) values of period is plotted against the mean period value for every oscillation identified from two or three microarray probe sets against the same gene. **(C)** Cumulative frequencies of period CV for oscillations with different periods calculated from **(B)**. **(D-G)** Comparison of the 8h cycling genes uncovered by the eigenvalue/pencil and the COSOPT method (Hughes et al., 2009). Venn diagram comparison of the number of 8h cycling genes identified via the eigenvalue/pencil or the COSOPT method **(D)**, the distributions of the periods of the dominant oscillations from the 39 commonly found 8h cycling genes **(E)**, the 6,255 8h genes only identified by the eigenvalue approach **(F)** or the dominant 1,430 8h genes identified by the eigenvalue approach (**G**). **(H-I)** Comparison of the 12h cycling genes uncovered by the eigenvalue/pencil and the RAIN method (Thaben and Westermark, 2014). Venn diagram comparison of the number of 12h cycling genes identified via the eigenvalue/pencil or the RAIN method with two p value cut-offs **(H)**, the distributions of the periods of the dominant oscillations from the 272 commonly found 12h cycling genes

with a p value cut-off of 0.01 **(I)**, the 266 commonly found 12h cycling genes with a p value cut-off of 0.05 **(J)** or the dominant 3,114 12h genes only identified by the eigenvalue approach (**K**). **(L-O)** Comparison of the 12h cycling genes uncovered by the eigenvalue/pencil and the JTK_CYCLE method (Hughes et al., 2010). Venn diagram comparison of the number of 12h cycling genes identified via the eigenvalue/pencil or the JTK_CYCLE method with two p value cut-offs **(L)**, the distributions of the periods of the dominant oscillations from the 27 commonly found 12h cycling genes with a p value cut-off of 0.01 **(M)**, the 45 commonly found 12h cycling genes with a p value cut-off of 0.05 **(N)** or the dominant 3,490 12h genes only identified by the eigenvalue approach (**O**). **(P-S)** Comparison of the 12h cycling genes uncovered by the eigenvalue/pencil and the ARSER method (Yang and Su, 2010). Venn diagram comparison of the number of 12h cycling genes identified via the eigenvalue/pencil or the ARSER method with two p value cut-offs **(P)**, the distributions of the periods of the dominant oscillations from the 272 commonly found 12h cycling genes with a p value cut-off of 0.01 **(Q)**, the 162 commonly found 12h cycling genes with a p value cut-off of 0.05 **(R)** or the dominant 3,218 12h genes only identified by the eigenvalue approach (**S**). **(T)** GO analyses revealing top-enriched SP_PIR_KEYWORDS and GOTERM_BP_FAT terms in the 760 dominant 12h genes.

Figure S3. 12h oscillations are transcriptionally-regulated independently from the 24h circadian rhythms in mouse liver, related to Figure 2.

(A) Heatmap of RPKM normalized mRNA expression for genes without embedded ~12h oscillations in wild-type mice in wild-type (WT) or *BMAL1*$^{-/-}$ (*BMAL1* KO) mice from a published RNA-Seq database at different CTs (Yang et al., 2016). **(B,C)** Heatmap **(B)** and representative mRNA expression **(C)** from wild-type (WT) and *CLOCK* mutant (Clockm) mice under constant darkness conditions calculated from a published micro-array database (Miller et al., 2007) and graphed as the mean ± SEM (n = 2). **(D-F)** We sought further evidence for the independence of 12h rhythmicity of gene expression from the circadian rhythm by examining global run-on sequencing (GRO-Seq) data in mouse liver across one diurnal cycle (Fang et al., 2014). GRO-Seq not only can accurately quantify nascent mRNA transcription, but also can identify actively transcribing enhancer

RNAs (eRNA), the level of which closely correlates with neighboring mRNA expression (Lam et al., 2014). We first confirmed that the 12h rhythm of mRNA expression is regulated at the transcription level **(D, E)**. Next, we reasoned that if the 12h rhythm is transcriptionally regulated independently from the circadian rhythm as speculated, we should identify examples of spatial segregation of 12h and 24h cycling eRNAs in the enhancer regions of the same gene that has both 24h and 12h oscillations superimposed at the mRNA level. As expected, we found examples of spatial segregation of 12h and 24h cycling eRNAs in *Acly*, *Fasn* and *Hspa8* genes, all of which have both 24h and 12h oscillations at the mature mRNA level **(F).** Detailed figure legends: RPKM normalized quantification of mouse hepatic RNA synthesis rate under a 12h L/D schedule calculated from a published Gro-Seq database (Fang et al., 2014). UCSC genome browser snapshots of H3K4me3, H3K4me1 and H3K27Ac levels (Koike et al., 2012) as well as Gro-Seq tracks from ZT1 to ZT22 at three-hour intervals are provided at the top. **(D)** UCSC genome browser snapshots (top) and quantification of the Gro-Seq signal of the RNA transcribed from the sense (pre-mRNA) and anti-sense (anti-sense RNA) strand of *Gfpt1*, *Sec23b* and *Eif2ak3* gene (bottom). Boxes indicate regions of RNA used for quantification. **(E)** Normalized quantification of additional 12h cycling mouse hepatic pre-mRNA level under a 12h L/D schedule. **(F)** UCSC genome browser snapshots of H3K4me3, H3K4me1 and H3K27Ac levels (Koike et al., 2012) as well as Gro-Seq tracks from ZT1 to ZT22 at three-hour intervals and quantification of the Gro-Seq signal of the pre-mRNAs and eRNAs transcribed from *Acly*, *Fasn* and *Hspa8* gene loci. Boxes indicate regions of RNA used for quantification.

Figure S4. Circadian clock-independent 12h rhythmicity of gene expression can be synchronized by the metabolic/ER stress cues, related to Figure 3 and 4.

(A) Raw microarray data and eigenvalue/pencil decomposition of 10 genes in forskolin-synchronized NIH3T3 cells (Hughes et al., 2009). **(B)** MEFs were treated with various doses of Tu for 2h and qPCR was performed on different genes 4h later. **(C, D)** MEFs were treated with Tu (25ng/ml) for 2h and qPCR was performed at different time points post-Tu shock. **(E)** MEFs were treated with a lower dose of Tu (15ng/ml) for 2h and qPCR was performed at different time points post-Tu shock. **(F, G)** MEFs were transfected with

different siRNAs and treated with Tu (25ng/ml) for 2h and qPCR was performed at different time points post-Tu shock for *Bmal1* **(F)** and *Xbp1* **(G)** genes. **(H)** Immunoblot analysis of BMAL1 and XBP1s in MEFs transfected with different siRNAs before Tu or GD treatment. **(I)** MEFs were transfected with different siRNAs and treated with Dex (100nM) for 30min and qPCR was performed at different time points post-Dex shock. (**J**) MEFs were transfected with different siRNAs and glucose starved for 2h and qPCR was performed at different time points post-GD. Gray boxes indicate the duration of Tu shock or GD. (**K**) Quantifications of both raw and polynomial-detrended single cell lineage recordings. (**L**) Calculated relative amplitudes of single cell oscillations with dominant periods between 11 to 14h. Data are graphed as the mean ± SEM (n=3).

Figure S5. XBP1s transcriptionally regulates the mammalian 12h clock., related to Figure 5.

(A) Heatmaps of proteins exhibiting 12h oscillation in mouse liver generated from a published SILAC database (Robles et al., 2014) (top) and of corresponding mRNA expression (Hughes et al., 2009) (bottom) at different CTs. **(B)** GO analysis revealing top-enriched SP_PIR_KEYWORDS in 12h and 24h cycling proteins. **(C)** Log_2 mean normalized level of proteins with a 12h period oscillation in mouse liver generated from a published SILAC database involved in different biological pathways (Robles et al., 2014). **(D-F)** Mice were entrained under 12L:12D schedule for 14 days before released into constant darkness. 36 hours later, mice were sacrificed at a 2h interval for a total of 48h. Representative western blot analysis from liver whole cell lysates **(D)** and quantification and eigenvalue/pencil decomposition **(E)** of key hepatic metabolic enzymes (n=3). **(F)** Quantification and eigenvalue/pencil decomposition of plasma insulin and glucose oscillations during the 48h period (n=3). Please note that both plasma glucose and insulin levels reveal robust circadian rhythmicity, with phases consistent with previously published results (Wang et al., 2011; Zhu et al., 2015). In addition, we observed an 1.55h phase delay between insulin and glucose oscillation, consistent with the kinetics of insulin release after an increase in blood glucose levels (Gerich, 2002). Intriguingly, neither plasma glucose nor insulin oscillations exhibited 12h rhythmicity. Further, insulin oscillation showed a more “pulsatile” pattern, consisting of superimposed oscillations with

periods of ~24h, 8h and 5h of relatively similar amplitudes; while the glucose oscillation is subtler with a strong circadian rhythmicity. The “pulsatile” insulin oscillating pattern across a diurnal cycle may be a macroscopic manifestation of 5~15min periodic insulin release (Porksen et al., 2002). These data indicate that mice kept under constant darkness conditions maintain a rhythmic feeding-fasting cycle. **(G)** Diagram of translational control of ATF4 under normal and ER stress conditions. Translation of the mammalian activating transcription factor-4 (ATF4) is regulated by two uORFs. When the eIF2-GTP-Met-tRNA ternary complex is abundant (in the presence of low levels of eIF2α phosphorylation) under normal conditions, the ribosomes initiate at uORF1 and frequently reinitiate at uORF2. As uORF2 overlaps with the ATF4 ORF, the translation of uORF2 suppresses the translation of ATF4. During ER stress, when the level of the ternary complex is reduced, the ribosome scans through uORF2 and initiates at the ATF4 initiation codon. Coding regions are shown as red rectangles, uORFs are shown as purple rectangles, ribosomes are shown in orange circles (60S subunit, large circle; 40S subunit, small circle). The ternary complex is shown as light blue circle. m^7G, cap structure. **(H)** Hepatic XBP1s binding to regulatory regions of key 12h metabolic genes under constant darkness conditions assayed by ChIP-qPCR (n=3~4) overlaid with RPKM normalized quantification of mouse hepatic RNA synthesis rate under a 12h L/D schedule calculated from a published Gro-Seq database (Fang et al., 2014) and BMAL1, CLOCK, PER2, H3K4me3, H3K4me1 and H3K27Ac cistromes (Koike et al., 2012). Amplicons of ChIP-qPCR and regions of RNA for quantification are illustrated by arrows of different color. **(I)** ChIP-qPCR of XBP1s on 4.5S RNA, *Per2* and *Cry2* promoter regions were used as negative controls (n=3). **(J-L)** ChIP-qPCR of XBP1s in 2h Tu-treated MEFs with different siRNA knock-down on *Sec23b* **(J)**, *Eif2ak3* **(K)** and *Hspa5* **(L)** genes (n=3). Data are graphed as the mean ± SEM for glucose and insulin quantification and ChIP-qPCR.

Figure S6. Spatio-temporal coordination of the 12h rhythm of hepatic metabolism, related to Figure 5 and 6.

(A) Key carbohydrate, nucleotide and lipid metabolic pathways having rate-limiting enzymes with 12h oscillations of expression in mouse liver are demonstrated in different colors. The phases of the oscillations of metabolic enzymes in corresponding metabolic

pathways are shown in the bottom right corner. In addition, the phases of the 12h rhythm of mRNA transcription based upon **Figure1 H** are also shown. Black-boxed phases indicate the phase of the larger peak that is often superimposed by the peak of the 24h circadian rhythm. Metabolic pathways lacking black-boxed phases indicate that the two peaks of the 12h rhythm are symmetrical and therefore suggest that they largely lack a superimposed circadian rhythm. Key rate-limiting enzymes with a 12h rhythm are numbered from 1 to 24 and numbers in blue indicate proteins whose corresponding mRNAs do not exhibit ~12h oscillation per the eigenvalue/pencil method. Please be noted that of the 18 NUDF family members, *Ndufa11*, *Ndufab1*, *Ndufb11*, *Ndufb2*, *Ndufb4* and *Ndufc2* do exhibit ~12h oscillation at the mRNA level (See **Table S1**). Further, the sub-cellular localizations (mitochondria, ER or nucleus) of different metabolic pathways are depicted by blue box, red box and yellow circle, respectively. **(B)** 12h rhythm of RBKS mRNA and protein expression is associated with the 12h oscillation of ribose levels in mouse liver. RBKS catalyzes the conversion from D-ribose to D-ribose 5-phosphate (top). Oscillations of *Rbks* pre-mRNA and eRNA transcription (middle left), mature *Rbks* mRNA expression and its eigenvalue/pencil deconvolution (middle right), RBKS protein level (bottom left) and ribose levels (bottom right) in mouse liver. **(C)** 12h rhythm of SUCLA2 mRNA and protein expression is associated with the 12h oscillation of succinyl-CoA level in mouse liver. SUCLA2 catalyzes the conversion from succinyl-CoA to succinate (top). Oscillations of *Sucla2* pre-mRNA transcription (middle left), mature *Sucla2* mRNA expression and its eigenvalue/pencil deconvolution (middle right), SUCLA2 protein level (bottom left) and succinyl-CoA levels (bottom right) in mouse liver. **(D-H)** Mice under *ad libitum* (n=7) or restricted feeding (n=8) conditions are housed in CLAMS system under a 12h L/D schedule. Averaged real-time food intake of mice under *ad libitum* **(D)** or restricted feeding **(E)** conditions. **(F)** Average daily food intake in light (ZT0~12) and dark (ZT12~ZT24) phase for mice housed under *ad libitum* and restricted feeding conditions. **(G-H)** Eigenvalue/pencil method deconvolution of RER data from 7 individual mice housed under *ad libitum* conditions **(G)** and from 8 individual mice housed under restricted feeding conditions **(H)**.

Figure S7. 12h CREMA is conserved in crustaceans and nematodes, related to Figure 7.

(A) RPKM normalized quantification of mouse hepatic mtDNA-encoded RNA synthesis rate under a 12h L/D schedule calculated from published Nascent-Seq dataset (Menet et al., 2012). UCSC genome browser snapshot of Nascent-Seq tracks across the 16.1 kb mouse mitochondrial genome. Protein-coding genes encoded on the positive (H) strand are shown in red while genes on the negative (L) strand are shown in blue. Boxes show UCSC tracks with higher magnification for specific regions. **(B)** mRNA levels of several mtDNA-encoded genes as calculated from a published microarray database (n=3) under a 12h L/D cycle (Eckel-Mahan et al., 2013). The data are double plotted for better visualization. Data are graphed as the mean ± SD. **(C)** qPCR analysis of four mtDNA-encoded genes under constant darkness conditions (n=3~7). Data are graphed as the mean ± SEM. **(D)** Raw data and eigenvalue/pencil decomposition of genes involved in mitochondrial gene regulation as calculated from the 48h microarray database (Hughes et al., 2009). **(E)** Log_2 (fold change to mean) for key *C. elegans* ortholog of mammalian 12h cycling ER and metabolism genes under temperature entrainment and free-run conditions. Two independent replicates (corresponding to experiment 3 and 4 in the original study) were shown. **(F)** List of top ten 12h cycling mouse genes identified by the eigenvalue/pencil method and their *C. elegans* orthologs with the status of 12h rhythmicity shown. Only genes with decay rate greater than 0.9 were selected. **(G)** Log_2 (fold change to mean) for *C. elegans* ortholog of mammalian top ten 12h cycling genes under temperature entrainment and free-run conditions. Two independent replicates (corresponding to experiment 3 and 4 in the original study) were shown. **(H)** List of top ten 24h cycling mouse genes identified by the eigenvalue/pencil method and their *C. elegans* orthologs with the status of 24h rhythmicity shown. Only genes with decay rate larger than 0.9 were selected. **(I)** Log_2 (fold change to mean) for *C. elegans* ortholog of mammalian top ten 24h cycling genes under temperature entrainment and free-run conditions. Two independent replicates (corresponding to experiment 3 and 4 in the original study) were shown.